Solid Oxide Electrochemical Doping Method for Preparation of Intelligent Oxide Materials

March 2003

KAI KAMADA

Graduate School of Science and Technology
KUMAMOTO UNIVERSITY

Acknowledgement

I wish to express my sincerest thanks to Prof. Y. Matsumoto for his valuable comments, discussions, suggestions and his constant encouragement during the period of my research project. Hearty thank are due to Prof. C. Hirayama and Dr. M. Koinuma, who acted as examiner of the dissertation, for their helpful and useful suggestions. Grateful acknowledgement is made to Mr. Y. Ogawa, Mr. K. Utou and Mr. M. Hirota for their technical assistance of instrumental measurements.

I kindly thank to Ms. Y. Ishikawa and Ms. K. Tahara as staffs of our laboratory for assistance to me in long duration. It is also great pleasure for me to show appreciation to Mr. S. Yamashita for the many fruitful discussions, proposals and his infinite efforts every time. I am deeply grateful to the co-researchers of my research projects, Mr. Y. Tanaka, Ms. N. Sakaguchi, Mr. S. Udo, Ms. M. Mukai, Mr. K. Maehara, and Ms. Y. Tsutsumi for their generous collaborations until now and in the near future.

I am also thankful to the Sasakawa Scientific Research Foundation, the Iketani Science Technology Foundation, and the Sagawa Foundation for Promotion of Frontier Science for the financial supports to my research project.

Finally, sincerely thanks to my parents and my three sisters for their constant encouragement, understanding and support.

Kai Kamada

Kumamoto
March, 2003

CONTENTS

Chapter 1

General Introduction

1.1. Significance of Cation Doping into the Oxide Materials

The physical and chemical properties of oxide materials depend significantly on the kind and amount of cations doped in the crystal lattice. Therefore, the cation doping into the oxide materials is very important for the development of functional materials such as semiconductors, dielectric ceramics, superconductors, etc. For instance, the doping of small amount strontium into Ba^{2+} sites in $BaTiO_3$ causes the shift of Currie point to higher temperature. In contrast, Ca doping into Ba^{2+} sites in $BaTiO_3$ shifts the Currie point to lower temperature. That is, Currie point of this ceramics can be easily manupilated by the doping of the other alkali earth cations. Moreover, Y^{3+} doping (< a few mol%) into Zr^{4+} sites in the low temperature ZrO_2 phase (monoclinic) results in the generation of oxygen vacancies in the lattice, which act as fast pass for oxide ion conduction, and stabilizes the high temperature phase (cubic) with extremely high oxide ion conductivity at even the medium temperature range.

For the conventional doping method, the doping has been carried out by heat treatment of a mixture containing the starting and dopant materials at high temperature (> 1000 °C). This technique is called "solid–state reaction" method. Recently, electrochemical doping in sintered oxide ceramics has been performed using solution electrolytes [1-4]. Some studies on electrochemical oxygen doping have been reported using anodic polarization of oxide ceramics in an alkaline solution. Bhavaraju and co-researchers [5] has discovered the transformation of insulator to superconductor using the same technique for copper complex oxide ceramics. Electrochemical Li^+ intercalation into Bi-Sr-Ca-Cu-O superconducting ceramics has been also performed by Fujiwara et al. in organic solvents with Li salts [6]. Ion exchange method is known as one of most important way to introduce the different cations into the materials. The target material is immersed into the molten salts or aqueous solutions containing dopant element, where dopant cation is substituted for cation in the target by the concentration gradient as a driving force. This technique is particularly used for the oxide materials with ionic conduction such as layered oxides [7-11] or glass materials [12-16], which include the mobile cation in interlayers or amorphous glass network, respectively. On the other hand, the ion injection technique [17-21] using gas phase ions at low pressure (about 10^{-4} Pa) is also a useful doping method of various metal and typical elements, and has been used for semiconductors, metals, some ceramics, etc.

1. 2. Principals of Solid Oxide Electrochemical Doping (SOED) Method

In contrast to the many routes to introduce the metal cations into oxide materials, we propose a new electrochemical technique of cation doping in this study. This is "Solid Oxide Electrochemical Doping (SOED) method [22]. Briefly described, the SOED method is a metal cation doping technique by using solid electrolytes with cationic conduction, where the cation injection into the target materials occurs at the interface of solid electrolyte and target materials under an electrical

field.

There are two main systems in the SOED method as shown in Fig. 1.1. In general, the SOED method employs an ion-conducting M-β"-Al_2O_3 (M = metal ion) [23-25] ceramics as a cation source. SOED 1 consists of an anode / M-β"-Al_2O_3 / target material / M'-β"-Al_2O_3 / cathode system, where the M^{n+} cation can be doped into the target material together with substitution of a cation (Q^{m+}) in the target so that the electrical neutrality is maintained in the target. Therefore, this doping model corresponds to "*electrosubstitution*" mechanism. In this case, both β"-Al_2O_3 block the conduction of the other charge carriers such as electrons, holes, and oxide ions. The following total reaction in the target will occur during the doping process together with electrochemical reaction at the anode (oxidation of metal into cation) and cathode (reduction of cation into metal):

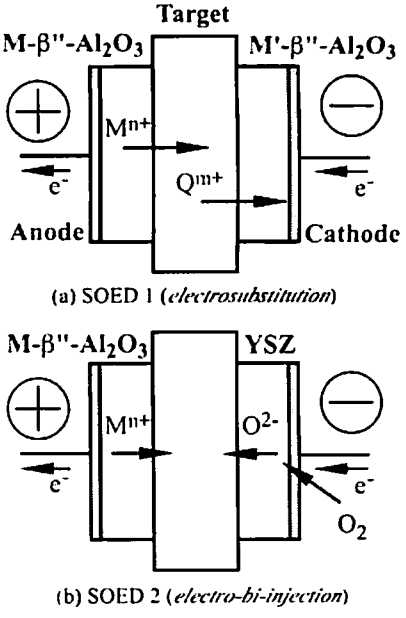

Figure 1.1. Models of ion migration in the main SOED systems.

$$mM^{n+}\ (M\text{-}\beta\text{''-}Al_2O_3) + nQ^{m+}\ (target) \rightarrow mM^{n+}\ (target) + nQ^{m+}\ (M'\text{-}\beta\text{''-}Al_2O_3).$$

SOED 2 consists of an anode / M-β"-Al_2O_3 / target / Y-stabilized ZrO_2 / cathode system, where oxide ion conducting Y-stabilized zirconia (YSZ) is employed instead of M'-β"-Al_2O_3 in the SOED 1. When an electrical field applies this system, the M^{n+} cation can be injected into the target together with the injection of an oxide ion so that electrical neutrality is maintained. Therefore, this doping is called "*electro-bi-injection*". The following reaction will proceed in the target together with the electrochemical reactions at the anode (oxidation of metal into cation) and cathode (O_2 reduction into O^{2-}):

$$2M^{n+}\ (M\text{-}\beta\text{''-}Al_2O_3) + nO^{2-}\ (YSZ) + target \rightarrow M_2\text{-}O_n\ (target).$$

As already stated, the maintenance of electrical neutrality in each parts of solid-state electrochemical cell is very important for ion migration (doping) in the SOED method.

1. 3. Advantages of the SOED method

Judging from the doping mechanisms of the SOED method, we can find some advantages of the present technique as follows. Table 1.1 indicates that the comparison of the characteristics of some doping methods. Although solid-state reaction technique is useful for preparation of the homogeneously doped materials, selective doping into the desired position of target is impossible. Moreover, high temperature above 1000 °C is required for doping and the doping point such as grain or grain boundary of ceramics is uniquely decided by the ionic valence and radius. In contrast, the ion implantation technique makes selective point doping possible, it needs high energy (kV – MV) for the ion acceleration, and the doping occurs only in the surface region of the substrate (< 10^6 m) [26]. The proposed technique has several merits compared with the usual method for doping. The doping amount can be preciously controlled by the electric charge. Various oxide materials such as single crystals, ceramics, and glass can be employed as a doping target, and many kinds of

metal cation, which is exchanged in β"-Al_2O_3 structure [27-30], can be used as a dopant. Furthermore, the SOED method allows for microarea doping if the tip of solid electrolyte with a small contact area is used during the electrolysis.

Table 1.1. Comparison of the techniques for cation doping.

	SOED	Ion Implantation	Ion Exchange	Solid State Reaction
Temperature	medium ~ 600 °C	room temp.	medium ~ 600 °C	high > 1000 °C
Atomsphere	ambient	in vacuum	ambient	ambient ~ high pressure
Point Doping	possible	possible (only surface)	impossible	impossible

1. 4. Objective and outline of the present work

The solid oxide electrochemical doping (SOED) method might become one of important applications of solid electrolyte such as a sensor [31, 32] and SOFCs [33-35] with a proton and oxide ion conducting solid electrolyte. In the present work, the advisability of metal cation doping by using the SOED method is investigated in detail, and the utility of this method is experimentally demonstrated. In particular, the investigations of the relationship between the doping condition (current, temperature, etc.) and the distribution of dopant in the target were the central topics of the present study, and then the ion migration mechanism was clarified. In some cases, the functionalities of doped materials by the SOED method were evaluated.

In Chapter 2, the electrosubstitution mechanism of the SOED 1 system was studied at temperature range 400 – 600 °C, where oxide ceramics was used as doping target. The results indicate that SOED 1 is a very useful method for doping various cations into all of the functional oxide ceramics independent of their conductive properties. Moreover, an improved system of SOED 1 to dope trivalent ions, which was difficult to incorporate to β"-Al_2O_3 structure [28, 36], was developed. As a result, the Bi^{3+} was doped into the grain boundaries of the ZnO ceramics under electrical bias.

In Chapter 3, electrochemical cation doping into the oxide ceramics has been carried out using SOED 2 method (electro-bi-injection). The SOED 2 method consists of the Anode / M-β"-Al_2O_3 / Ceramics / YSZ / Cathode electrolysis system, where the metal cation M and oxide ion are simultaneously injected into the oxide ceramics so that electrical neutrality is maintained in the ceramics. In general, graded doping occurred at a relatively high temperature.

In Chapter 4, the pinpoint doping, which is one of most important feature in the SOED method, was performed by using the β"-Al_2O_3 microelectrode. In the case of Ag doping into the borosilicate glass, the distribution of silver occurred in a hemispherical shape with its center at the Ag-β"-Al_2O_3 / glass microcontact. The diameter of doped area in the glass strongly depended on the applied electric charge. As a result, the pinpoint doping on a 10^2 μm scale was accomplished using the SOED method.

In Chapter 5, as one application of the pinpoint doping by the SOED method, electrochemical design of metal distribution in the surface of an alkali borosilicate glass was carried out using an ion-conducting Ag-β"-Al_2O_3 microelectrode. Scanning Ag-β"-Al_2O_3 microelectrode under applying an electric field caused the patterned Ag-distribution in the glass surface.

It seems that the doping amount is related to the electric charge during the electrolysis because the SOED method is electrochemical technique. Hence, the quantitative analysis of metal cation doping by the SOED method was also performed under galvanostatic doping conditions. In Ag-doping into alkali borate glass, the measured dopant amount closely matched the theoretical value. In contrast, current efficiencies of Na-doping into $Bi_2Sr_2CaCu_2O_y$ ceramics depended on the applied constant current. While the high efficiencies of above 80 % were achieved at a low current, the

relatively low efficiencies were obtained at a high current. These results were stated in Chapter 6.

Finally, Chapter 7 summarized the present results, and states the future view of the SOED method.

1. 5. References

[1] J.C. Bennett, M. Olfert, G.A. Sholz, F.W. Boswell, *Phys. Rev.* **B44**, 2727 (1991).

[2] J.C. Grenier, A. Wattiaux, A. Demourgues, M. Pouchard, P. Hagenmuller, *Solid State Ionics* **63-65**, 825 (1993).

[3] L. Chen, A. van Zomeren, J. Schoonman, *Solid State Ionics* **50**, 55 (1992).

[4] A.M. Andersson, C.G. Granqvist, Z.G. Ivanov, *J. Alloys Comp.* **195**, 343 (1993).

[5] S. Bhavaraju, J.F. DiCarlo, I. Yazdi, A.J. Jacobson, H.H. Feng, Z.G. Li, P.H. Hor, *Mater. Res. Bull.* **29**, 735 (1994).

[6] M. Fujiwara, M. Nakanishi, Y. Kusano, T. Fujii, J. Takada, Y. Takeda, Y. Ikeda, *Physica C* **279**, 219 (1997).

[7] R. Abe, M. Hara, J.N. Kondo, K. Domen, *Chem. Mater.* **10**, 1647 (1998).

[8] T. Sumida, Y. Takahara, R. Abe, M. Hara, J.N. Kondo, K. Domen, M. Kakihana, M. Yoshimura, *Phys. Chem. Chem. Phys.* **3**, 640 (2001).

[9] T. Sasaki, F. Kooli, M. Iida, Y. Michiue, S. Takenouchi, Y. Yajima, F. Izumi, B.C. Chakoumakos, M. Watanabe, *Chem. Mater.* **10**, 4123 (1998).

[10] M. Ohashi, *Mol. Cryst. Liq. Cryst.* **341**, 265 (2000).

[11] Y. Fujishiro, S. Uchida, T. Sato, *Int. J. Inorg. Mater.* **1**, 67 (1999).

[12] M.A. Villegas, J.M. Fernandez Navarro, S.E. Paje, J. Llopis, *Phys. Chem. Glasses* **37**, 248 (1996).

[13] M. Dubiel, S. Brunsch, U. Kolb, D. Gutwerk, H. Bertagnolli, *J. Non-Cryst. Solids* **220**, 30 (1997).

[14] B. Roy, H. Jain, S. Roy, D. Chakravorty, *J. Non-Cryst. Solids* **222**, 102 (1997).

[15] M. Abou-El-Leil, A.R. Cooper, *J. Am. Ceram. Soc.* **62**, 390 (1979).

[16] M.H. Shaaban, A.A. Ahmed, A.R. Cooper, *Phys. Chem. Glasses* **40**, 34 (1999).

[17] G. Dernaley, *Ion Implantation*, North-Holland, Amsterdam (1973).

[18] A. Nakajima, T. Futatsugi, H. Nakao, T. Usuki, N. Horiguchi, N. Yokoyama, *J. Appl. Phys.* **84**, 1316 (1998).

[19] L.C. Nistor, J. van Landuyt, J.D. Barton, D.E. Hole, N.D. Skelland, P.D. Townsend, *J. Non-Cryst. Solids* **162**, 217 (1997).

[20] M.T. Pham, W. Matz, H. Seifarth, *Anal. Chim. Acta* **350**, 209 (1997).

[21] G.W. Arnold, J.A. Borders, *J. Appl. Phys.* **48**, 1488 (1977).

[22] Y. Matsumoto, *Solid State Ionics* **100**, 165 (1997).

[23] J.L. Sudworth, A.R. Tilley, *The Sodium Sulfer Battery*, Chapman and Hall, New York (1985).

[24] J.L. Sudworth, P. Barrow, W. Dong, B. Dunn, G.C. Farrington, J.O. Thomas, *MRS Bull.* **25**, 22 (2000).

[25] B. Dunn, G.C. Farrington, J.O. Thomas, *MRS Bull.* **14**, 22 (1989).

[26] S. Tanaka, *Bull. Ceram. Soc. Jpn.* **25**, 532 (1990).

[27] G.S. Rohrer, G.C. Farrington, *J. Solid State Chem.* **85**, 299 (1990).

[28] G.S. Rohrer, G. C. Farrington, *Chem. Mater.* **1**, 438 (1989).

[29] C.K. Kuo, P.S. Nicholson, *Solid State Ionics* **69**, 163 (1994).
[30] A. Tan, C.K. Kuo, P.S. Nicholson, *Solid State Ionics* **45**, 137 (1991).
[31] H. Iwahara, *Solid State Ionics* **86-88**, 9 (1996).
[32] H. Iwahara, *Solid State Ionics* **77**, 289 (1995).
[33] T. Ishihara, H. Matsuda, Y. Takita, *J. Am. Chem. Soc.* **116**, 3801 (1994).
[34] G.A. Topsett, N.M. Sammers, O. Yamamoto, *J. Am. Ceram. Soc.* **80**, 3181 (1997).
[35] M. Mori, T. Abe, H. Itoh, O. Yamamoto, *Solid State Ionics* **74**, 157 (1994).
[36] S. Sattar, B. Ghosal, M.L. Underwood, H. Mertwoy, M.A. Saltzberg, W.S. Frydrych, G.S. Rohrer, G.C. Farrington, *J. Solid State Chem.* **65**, 231 (1986).

Chapter 2

Cation Doping into the Oxide Ceramics by the SOED 1 Method

2.1.Introduction

Many studies of doping into oxide ceramics have been made in order to improve their properties. It is well known that Ag doping improves the superconducting properties of $YBa_2Cu_3O_y$ (YBCO) ceramics. In general, it is believed that Ag diffuses in the grain boundaries of as a metal during thermal doping. In our laboratory, it was found that a small amount of Ag substitutes for Cu in the YBCO bulk [1], and that Ag^+ conduction is relatively high in the grain boundaries in superconducting ceramics at high temperature [2, 3]. These results suggest that a small amount of Ag substitutes for Cu and migrates in the grain boundaries as an ion (Ag^+) during the doping.

In the present section, an electrochemical cation doping into high temperature superconducting oxide ceramics ($YBa_2Cu_3O_y$, $Bi_2Sr_2CaCu_2O_y$) was performed using the SOED 1 system, and the doping mechanism of the SOED 1 system was clarified. The doping points (the grains or the grain boundaries) in the ceramics can be controlled by the current density during the electrolysis. In the most cases, cation was selectively doped into the grain boundaries of oxide ceramics, while the cation incorporation into crystal lattice was observed at high current density dependent on the kind of dopant. In addition, an improved SOED system was proposed in order to dope trivalent cation into oxide ceramics, and then the utility of this system was demonstrated for Bi^{3+} doping into ZnO ceramics. We have also studied about the electrosubstitution reaction at the solid-solid interface between metal or metal compounds anode and Na-β"-Al_2O_3 to elucidate an electrochemical reaction at the anode / M-β"-Al_2O_3 interface in the SOED system.

2. 2. Various Cations doping into the $YBa_2Cu_3O_y$ (YBCO) Ceramics by the SOED 1 system

2. 2. 1. Experimental

In the present experiment, a YBCO superconductor was used as the oxide ceramics. Y_2O_3, $BaCO_3$, and CuO were used as the starting materials for the preparation of the YBCO powder. The mixture was heated at 930 °C for 10 h, and then reground, followed by reheating under the same conditions. The pelle sample (thickness, 1.5 mm; surface are, 1.5 cm^2) of the YBCO was prepared by pressing the powder under 1000 kg/cm^2 and heating 930 °C. The solid electrolytes of M-β"-Al_2O_3 (M = Na^+, Ag^+, K^+, Ca^{2+}, Sr^{2+}, and Zn^{2+}) were prepared by the substitution of M in Na-β"-Al_2O_3 as previously reported [4-6]. The presence of M in these electrolytes was confirmed by electron probe microanalysis (EPMA). The electrochemical doping

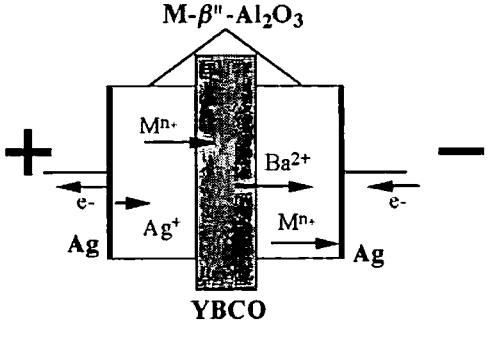

Figure 2.1. Model of the SOED 1 system for cation doping into YBCO ceramics.

by the SOED 1 system was carried out for 1 under constant current (< 1 mA) using the experimental setup schematically shown in Fig. 2.1. During the doping, the electrochemical oxidation Ag to Ag^+ occurs at the Ag anode, while the electrochemical reduction from M^{n+} to M occurs at the Ag cathode. The apparent contact area in the YBCO / M-β"-Al_2O_3 interface was 0.25 cm^2. The electrolysis was done at 400 – 600 °C. After the electrolysis the distribution state of the dopants in the cross section of the YBCO ceramics was analyzed using EPMA. The composition and/or crystal structure of the doped samples were based on an analysis of their X-ray diffraction patterns. The resitivities of the doped YBCO samples were measured by a conventional DC four-probe method, using a 10 mA DC current. Their AC susceptibilities were also measured using an AC inductance bridge.

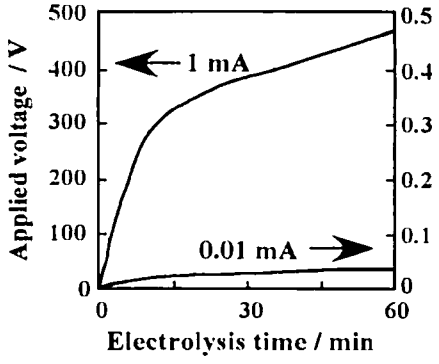

Figure 2.2. Dependencies of the applied voltage for Ag doping into YBCO ceramics on the electrolysis time under constant currents.

2. 2. 2. Results and discussion

Figure 2.2 indicates the dependencies of the applied voltage on the electrolysis time for Ag doping into YBCO ceramics using Ag-β"-Al_2O_3 under constant currents at 600 °C. The applied voltage increased with an increase in the electrolysis time, and was less than a few volts and few hundred volts for 0.01 mA and 1 mA, respectively. EPMA elemental distribution maps of the cross section of cathode side Ag-β"-Al_2O_3 after Ag-doping is shown in Fig. 2.3. Only Ba was always observed in the cathode β"-Al_2O_3 electrolyte after the electrolysis under all conditions and was independent of the kind of dopants. This indicats that only Ba^{2-} in YBCO moves during the electrolysis. Simultaneously, it is suggested that the bond strength of Ba^{2+} in the YBCO structure is the weakest of all cations in the YBCO. In principle, the following electrochemical reactions will occur at both sides of the M-β"-Al_2O_3 / YBCO / M-β"-Al_2O_3 interfaces.

$$xM^{n+} + nxe^- + YBa_2Cu_3O_y \rightarrow YBa_2M_xCu_3O_y \text{ (anode side)}$$

$$YBa_2Cu_3O_y \rightarrow (nx/2)Ba^{2+} + nxe^- + YBa_{2-nx/2}Cu_3O_y \text{ (cathode side)}$$

The dopant M^{n+} in the $YBa_2M_xCu_3O_y$ will diffuse in the YBCO ceramics under an electric field.

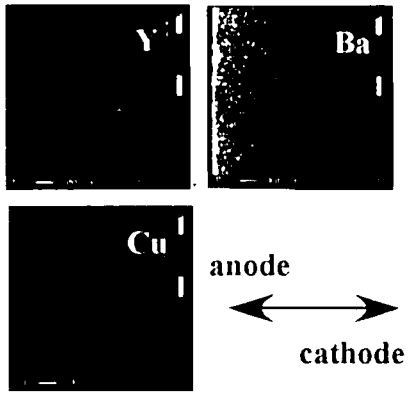

Figure 2.3. EPMA elemental distribution maps of the cross section in cathode side Ag-β"-Al_2O_3 after Ag doping at 1 mA for 60 min.

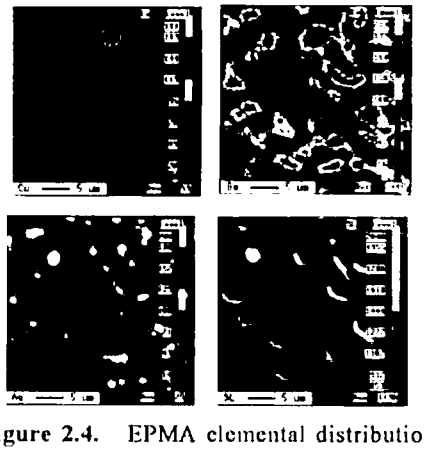

Figure 2.4. EPMA elemental distribution maps of the cross section in YBCO after Ag doping at 0.01 mA for 60 min.

After the electrolysis at a current lower than about 0.01 mA (at low applied voltage), the dopant was uniformly distributed over the entire sample on a macro-scale, while it exists in the grain boundaries and the pores on a micro-scale, but not in the bulk. Figure 2.4 shows the typical distribution maps of the element and SEM micrograph of the cross section of the Ag doped YBCO at 0.01 mA. The YBCO scarcely decomposed according to the X-zray analysis at low current, as shown in (b) of Figure 2.5, which shows some typical X-ray diffraction patterns of the doped and undoped YBCO samples. This indicates that all of the dopant cations smoothly diffuse into the grain boundaries of the YBCO ceramics together with the substitution for Ba^{2+} as illustrated in Figure 2.6 (a). This phenomenon is due to the grain boundary ionic conduction (diffusion) that is much higher than that of the bulk for the oxide ceramics.

On the other hand. two type phenomena were observed during the electrolysis at currents higher than about 0.01 mA (at high applied voltage). One is the grain boundary diffusion of the dopants together with the destruction of the YBCO. This occurred for all dopants except Ca^{2+}. In this case, a large amount of the dopants was observed

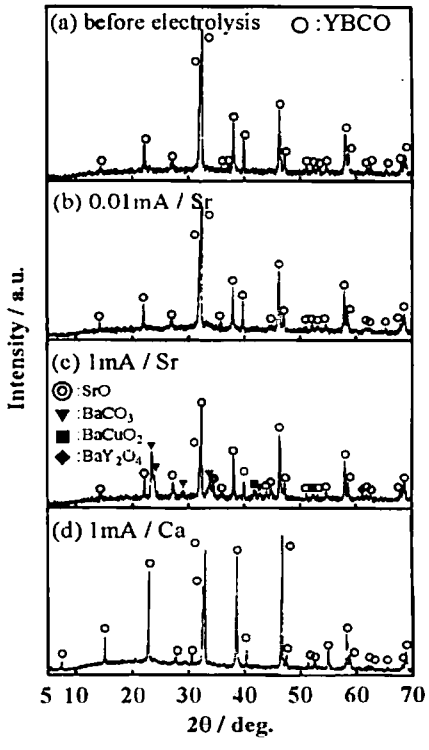

Figure 2.5. Typical X-ray diffraction patterns of the doped and undoped YBCO at 600 °C. (a), (b), and (c) are the diffraction patterns of the undoped sample, the Sr doped sample at 0.01 mA, the Sr-doped sample at 1 mA, and the Ca-doped sample at 1 mA, respectively.

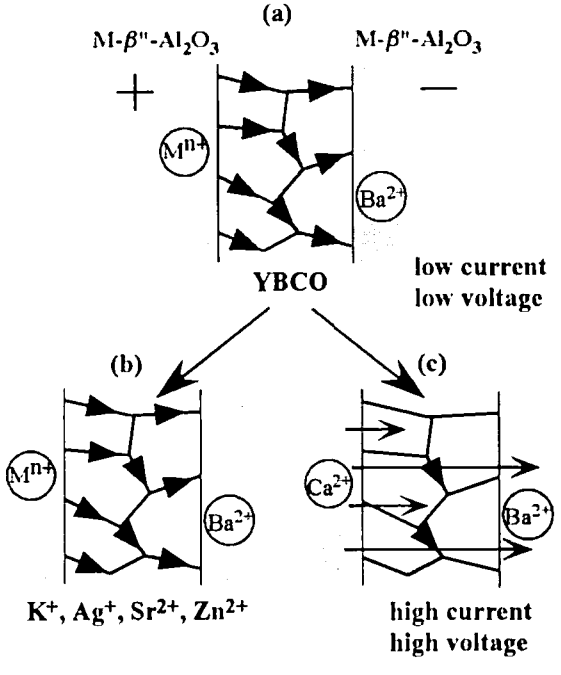

Figure 2.6. Models of the diffusion paths. M^{n+} smoothly diffuses in the grain boundaries of the YBCO ceramics under low current and/or low applied bias voltage (a). Under high current and/or high applied bias voltage, M^{n+} (K^+, Ag^+, Sr^{2+}, Zn^{2+}) moves in the grain boundaries together with the destruction of the YBCO (b), while Ca^{2+} diffuses in the bulk without the same destruction(c).

together with impurities such as M (metal for Ag), MO (for Sr and Zn), CuO (for Ag and Zn) $BaCO_3$, BaY_2O_4 and $BaCuO_2$ produced by the destruction of the YBCO at the grain boundaries, as shown in Fig. 2.5(c) for the Sr doped YBCO. These impurities will be produced by the destruction of the $YBa_2M_xCu_3O_y$ and $YBa_{2-nx/2}Cu_3O_y$ having large x value. This doping model is illustrated in Fig. 2.6(b).

The second phenomenon is the bulk diffusion of Ca^{2+} which is very surprising. Figure 2.7 shows the distribution maps of the element and SEM micrograph of the cross section of the Ca doped YBCO at 1 mA. Ca uniformly existed over the entire bulk of the YBCO. Moreover, no destruction of YBCO occurred during the electrolysis according to the X-ray analysis as shown in Fig. 2.5(d). That is, Ca^{2+} moves together with substitution for Ba^{2+} in the YBCO structure whose model is illustrated in Fig. 2.6(c).

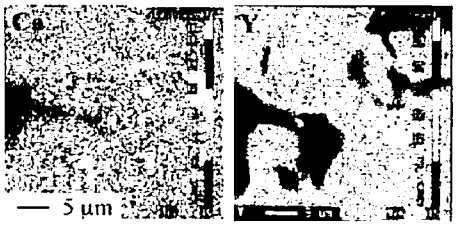

Figure 2.7. Distribution maps of the element of the cross section of the Ca-doped YBCO at 1mA.

The amounts of Ca doped in the samples were analyzed by EPMA. Two areas of the samples were analyzed in the cross section of the doped samples. One is a plane analysis to determine the amount of Ca in all of the parts, i.e., grain bulk and grain boundaries in the sample. The other is a pinpoint analysis to determine mainly the amount of Ca only in the grain bulk. Therefore, the amounts of Ca in each area of the samples can be easily calculated from the above data. Figure 2.8 shows the amount of the Ca (a) and the doping current efficiency (b) as a function of the electrolysis time. The doping was carried out at 1 mA at 600 °C. The amount of Ca saturated to a constant level at about 30 min independent of the doping area, and therefore, the current efficiency decreases with the electrolysis time. This indicates that the Ca^{2+} ion moves through the YBCO ceramics into the cathodic side Ag-β"-Al_2O_3 after saturation of the doping amount. In fact, Ca was detected in the cathodic side Ag-β"-Al_2O_3 after electrolysis for 30 min. It should be noted that the current efficiency in the grain boundaries is large compared with that in the grain bulk at the initial time electrolysis (about a few minutes). That is, initially the Ca doping occurs in the grain boundaries even at high current electrolysis, and then the grain bulk doping occurs.

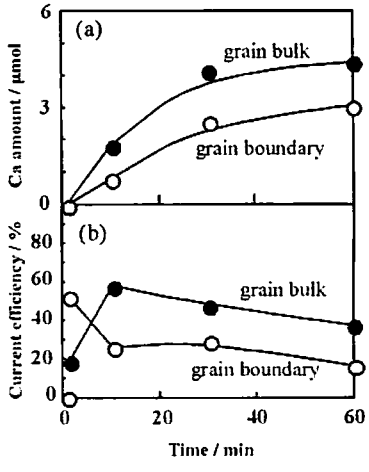

Figure 2.8. Amounts of Ca (a) in the doped samples and their current efficiencies (b) as a function of the electrolysis time.

The lattice constants decreased from a = 0.381 nm, b = 0.389 nm, c = 1.168 nm for the present pure YBCO to a = 0.373 nm, b = 0.385 nm, c = 1.152 nm for the Ca doped YBCO at 1 mA for 1 h. No substitution of Ca^{2+} for Ba^{2+} occurred due to heat-treatment at 600 °C if no bias voltage is applied. It depends on the dopants but not Ba^{2+} as to whether or not the bulk diffusion occurs, because Ba^{2+} always moves independent of the kind of dopants. Ca^{2+} will easily diffuse via the Ba^{2+} site to the YBCO structure, since its ionic size is relatively small and has the same coordination number as Ba^{2+}.

Figure 2.9 shows the unit cell volume of the $YBa_{2-x}Ca_xCu_3O_y$ as a function of x. In this figure, the results reported by Zhao et al. [7] where $YBa_{2-x}Ca_xCu_3O_y$ is prepared by conventional solid state reaction are shown. The composition and the lattice constants of the present Ca-doped samples were

analyzed by XRD and EPMA, respectively. The results for the samples doped at 0.01 mA and 1 mA for one hour are also plotted. It should be noted that the cell volumes of the present doped samples are much smaller than those in Ref. [7] for samples with the same x value. This is remarkable for the sample doped at 1 mA, as shown in Fig. 2.9. The present Ca-doped samples always had small amounts of Ba vacancies according to the EPMA. Therefore, the main cause for the decrease in the cell volume will be based on the Ba vacancy produced during the Ca electro-substitution. The critical temperatures (Tc) for the samples doped at various currents were determined by the ac susceptibility measurement. The Tc was about 92 K for all of the samples and was independent of the unit cell volume.

The dependence of the resistivity on temperature for the present YBCO ceramics, which reflects both the superconducting properties of the bulk and the grain boundary. The T_c in the ac susceptibility measurement scarcely changed for the Ca doped (bulk) and the Ag doped (grain boundary without the destruction) YBCO samples. Therefore, a small shift in the resistive T_c and a decrease in the resistivity at room temperature for the Ag doped YBCO due to the improvement in the grain boundaries by Ag [1, 2].

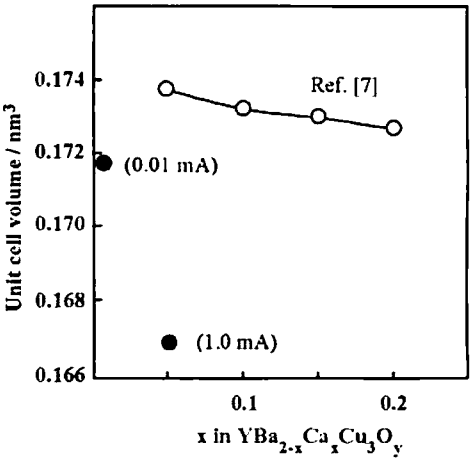

Figure 2.9. Unit cell volume as a function of the doped x in $YBa_{2-x}Ca_xCu_3O_y$.

2. 3. Cation doping into $Bi_2Sr_2CaCu_2O_y$ ceramics using the SOED 1 system

The mechanism for the various cation doping into the superconducting $YBa_2Cu_3O_y$ ceramics by the SOED method has been discussed in above section. On the other hand, the Bi-based cuprate oxide superconductor, $Bi_2Sr_2CaCu_2O_y$, is expected to one of the candidates with high potential for practical applications [8]. In this section, the SOED 1 tests in the $Bi_2Sr_2CaCu_2O_y$ ceramics were carried out using the various metal cation as a dopant, and the relation between the kind of the dopant and its distribution state in the ceramics is clarified.

2. 3. 1. Experimental

In the present experiment, $Bi_2Sr_2CaCu_2O_y$ (BSCCO, Dowa Kogyo Co., Ltd.) was used as the starting powder. The pellet ceramic samples (thickness: 1.5 mm, surface area: 0.8 cm^2) were prepared by cold isostatic pressing (CIP) and heating at 830 °C for 10 h. The solid electrolytes of M- β"-Al_2O_3 were prepared by the substitution of M (Ag, K, Zn) using Na- β"-Al_2O_3 (Nihon Tokushu Togyo Co., Ltd.). The apparent contact area in M- β"-Al_2O_3 / BSCCO / Na- β"-Al_2O_3 system was 0.4 cm^2. The electrochemical doping was carried out for 180 min under constant current density of 0.25 mA/cm^2 at 400 °C using the experimental setup schematically shown in Fig. 2.10. After the electrolysis, the distribution state of the dopants and crystal structure in a cross section of doped BSCCO samples were analyzed using electron probe microanalysis (EPMA) and X-ray microarea diffractometer, respectively. The BSCCO lattice constants were calculated from XRD patterns using silicon powder as a standard material. The AC susceptibilities of the doped samples was also measured

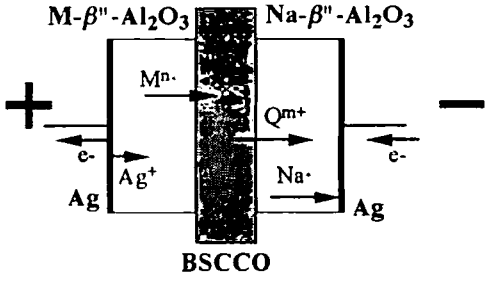

Figure 2.10. Model of the SOED 1 system for cation doping into BSCCO ceramics.

using an AC inductance bridge to determine the critical temperature (T_c).

2. 3. 2. Results and discussion

The basic migration mechanism is illustrated in Fig. 2.10 in the present SOED method (SOED 1 type). As a result, M^{n+} is substituted for Q^{m+} under an electrical force in the BSCCO ceramics analogous to cation doping into YBCO as state already. Under present condition, no cation doping through the M- b"-Al_2O_3 into the BSCCO occurred in the absence of bias at 400 °C.

Experimental results for doping with various cation are listed in Table 2.1. These results demonstrate that SOED 1 method is also a very useful technique for doping various cation into BSCCO ceramics. In general, the doping occurred only in the grain boundaries of the BSCCO, while Zn^{2+} was doped into the bulk of the grains (crystal lattice) as well as the grain boundaries under same condition. The applied voltage under 0.25 mA/cm^2 at 400 °C increased with an increase in the electrolysis time. The applied voltage for the case of Zn^{2+} was somewhat larger than that for the cases of Ag^+ and K^+. This indicates that the doping was easier for the monovalent cation than for divalent one because the ionic conductivity of the monovalent cation in the oxide ceramics is higher than that of the divalent one. Only Sr was always observed in the cathode Na- β"-Al_2O_3 electrolyte after the electrolysis under all conditions and was independent of the kind of dopants. This indicates that only the Sr^{2+} ion (Q^{m+} in Fig. 2.10) in the BSCCO ceramics moves during the electrolysis. Simultaneously, it is suggested that Sr^{2+} has a relatively weak bond strength in the BSCCO structure as well as Ba^{2+} in YBCO.

After the electrolysis, all of dopants such as Ag, K and Zn were uniformly distributed over the entire BSCCO sample, according to EPMA analysis. Two types of phenomena were observed during the electrolysis on a microscale. One is the grain boundary diffusion of Ag^+ and K^+, where the dopants were detected in the grain boundaries and the pores of the BSCCO ceramics, but not in the bulk. In these cases, a small amount of impurity phase such as Ag metal (for Ag^+ doping) or K_2CO_3 (for K^+ doping) and CuO (produced by the destruction of BSCCO at the grain boundaries) was detected in the cross section of the doped BSCCO ceramics, according to their XRD patterns. This indicates that the monovalent cations (Ag^+ and K^+) smoothly diffuse into the grain boundaries of the BSCCO ceramics together with the substitution for Sr^{2+} as illustrated in Fig. 2.11(a). This phenomenon is due to the grain boundary ionic conduction (diffusion) that is much higher than that of the bulk for the oxide ceramics.

Table 2.1. Experimental results in the various cation doping into the BSCCO ceramics by the SOED method

Doping cation	Applied Voltage[a)]	Main doping point[b)]	Lattice constant	
			a / nm	*c* / nm
undoped			0.539	3.075
Ag^+	500V	GB	0.540	3.075
K^+	450V	GB	0.539	3.073
Zn^{2+}	850V	G, GB	0.536	3.061

a) measured after 180 min electrolysis.
b) G and GB represent grain and grain boundary, respectively.

The second phenomenon is the bulk diffusion of Zn^{2+} in the BSCCO as already stated. As shown in Fig. 2.11(b), Zn uniformly existed over the entire bulk of the BSCCO. That is, Zn^{2+} migrates in the grain bulk together with substitution for Sr^{2+} in the BSCCO without any destruction of the crystal structure whose model is illustrated in Fig. 2.11(b). The tetragonal lattice constants decreased from a = 0.539 nm, c = 3.075 nm for the present pure BSCCO to a =

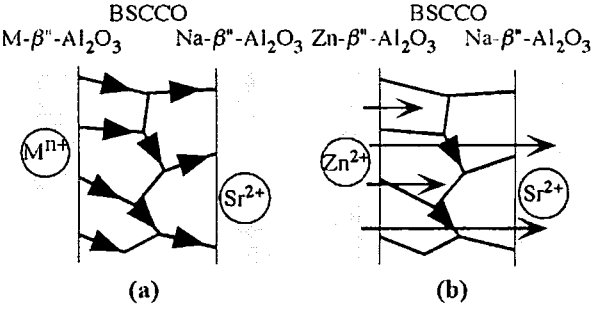

Figure 2.11. Models of the diffusion paths. M^{n+} (K^+, Ag^+) diffuses in the grain boundaries of the BSCCO ceramics (a), while Zn^{2+} diffuses in the bulk as well as grain boundaries (b).

0.536 nm, c = 3.061 nm for the Zn-doped BSCCO as shown in Table 2.1. The main cause for the decrease in the lattice constant will be based on the Sr vacancy produced during the electrolysis. Whether or not the bulk diffusion occurs depends on the dopants, but not Sr^{2+}, because Sr^{2+} always moves independent of the kind of dopants. Zn^{2+} will easily diffuse via the Sr^{2+} site to the BSCCO structure, since Zn^{2+} has a relatively small ionic size and same valence with the Sr^{2+}. This tendency was in harmony with the case of Ca doping into the $YBa_2Cu_3O_y$ (YBCO) ceramics, where Ca^{2+} has a relatively small ionic size and same valence was substituted for Ba^{2+} site under an electrical force, but the other cations (Na^+, K^+, Ag^+, Sr^{2+}) were doped only in the grain boundaries of the YBCO ceramics. The critical temperatures (T_c) for the samples doped with various cations were determined by the AC susceptibility. The T_c was about 62 K for all of the doped sample. This result indicates that the cation doping by the SOED method resulted in no significant effect on T_c because the amount of dopant was very small (10^{-2} mol%) under present condition.

2.4. Trivalent cation doping into oxide ceramics using a new type SOED 1 system

In the SOED method, the doping of trivalent cations (M^{3+}) into the ceramics was very difficult, although many kinds of monovalent and divalent cations (M^+, M^{2+}) can be doped into all oxide ceramics. There are two main reasons for the impossibility in M^{3+} doping. One is the difficulty in the movement of the M^{3+} ions through the oxide [9]. The other is the difficulty in the preparation of the pure M^{3+}-β"-Al_2O_3 [10, 11] compared to M^+, M^{2+}-β"-Al_2O_3 [4, 5, 12, 13]. The residual Na^+ ion preferentially moves rather than the M^{3+} ion if the M^{3+} ion is not completely substituted for Na^+ during the preparation. In this section, a new type SOED 1 method, which consists of the Ag(s) / Ag^+ (Na-β"-Al_2O_3) / Bi_2O_3 / ZnO / Na^+ (Na-β"-Al_2O_3) / Pt electrolysis system (Fig. 2.12), has been developed and the Bi^{3+} doping into the ZnO ceramics has been accomplished.

2.4.1 Experimental

Figure 2.12 shows a model of the present SOED system for the Bi^{3+} doping into the ZnO ceramics. In the present experiment, Ag and Pt plates were used as the anode and cathode, respectively. The pure ZnO powder (Mitsui Kinzoku Kogyo Co., Ltd.) was pressed under 2000 kg cm^{-2} using cold isostatic pressing (CIP) and heated at 1100 °C to prepare a pellet (thickness: 1.0 mm). The Bi_2O_3 pellet sample (a-type structure, thickness: 1.0 mm) was prepared by heating $Bi_2(CO_3)O_2$ at 700 °C. The Na-β"-Al_2O_3 pellet (Nihon Tokushu Togyo Co., Ltd., thickness: 2.0 mm) was used as the solid electrolyte. The electrochemical doping was carried out for 2-10 h under constant current (50 μA) at 600 °C using the experimental setup schematically shown in Fig. 2.12. The apparent contact area for the Bi_2O_3 / ZnO / Na-β"-Al_2O_3 system was 0.4 cm^2. The good contact in the ceramic/ceramic interfaces which avoids the current inhomogeneities, has been achieved by rubbing the ceramics strongly each other. After the electrolysis, the distribution state of the dopants in a cross section of all the pellets (Bi_2O_3, ZnO, Na-β"-Al_2O_3) was analyzed using electron probe microanalysis (EPMA). The crystal structure of each pellet was analyzed from X-ray diffraction (XRD) patterns. After the electrolysis, an In-Ga alloy was attached

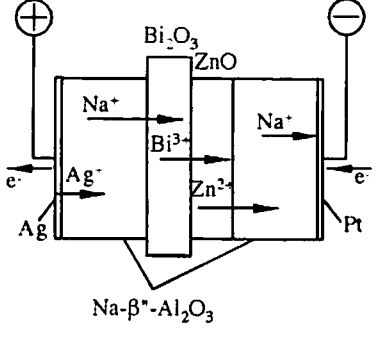

Figure 2.12. Model of the ion migration for the new type SOED method.

to both sides of the Bi-doped ZnO pellet and then the current-field curve as the varistor property was measured at room temperature.

2.4.2 Results and discussion

The following total reactions will occur during the electrolysis.

$nAg \rightarrow nAg^{+}(Na\text{-}\beta''\text{-}Al_2O_3) + ne^{-}$ (Ag anode) (1)

$nNa^{+}(Na\text{-}b''\text{-}Al_2O_3) \rightarrow nNa^{+}(Bi_2O_3)$ ($Na\text{-}\beta''\text{-}Al_2O_3$ / Bi_2O_3 interface) (2)

$n/3Bi^{3+}(Bi_2O_3) \rightarrow n/3Bi^{3+}(ZnO)$ (Bi_2O_3 / ZnO interface) (3)

$n/2Zn^{2+}(ZnO) \rightarrow n/2Zn^{2+}(Na\text{-}\beta''\text{-}Al_2O_3)$ (ZnO / $Na\text{-}b''\text{-}Al_2O_3$ interface) (4)

$nNa^{+}(Na\text{-}\beta''\text{-}Al_2O_3) + ne^{-} \rightarrow nNa$ (Pt cathode) (5)

Na^{+} in $Na\text{-}\beta''\text{-}Al_2O_3$ is injected into Bi_2O_3 (Eq. (2)) under electrical force. Electrochemical Bi doping into ZnO ceramics occurs together with the substitution for Zn^{2+} during the electrolysis (Eqs. (3) and (4)).

Na deposited at the Pt cathode immediately reacts with CO_2 in the air to form Na_2CO_3 which was detected by an XRD analysis. According to the EPMA measurement, Ag, Na, Bi, and Zn were detected in the $Na\text{-}\beta''\text{-}Al_2O_3$ (anode side), Bi_2O_3, ZnO and $Na\text{-}\beta''\text{-}Al_2O_3$ (cathode side) pellets after the electrolysis, respectively. No doping occurred in any of the pellets when no current flowed. Therefore, it is concluded that the ion migrations illustrated in Fig. 2.12 and Eqs. (1)–(5) occur in the present SOED system during the electrolysis.

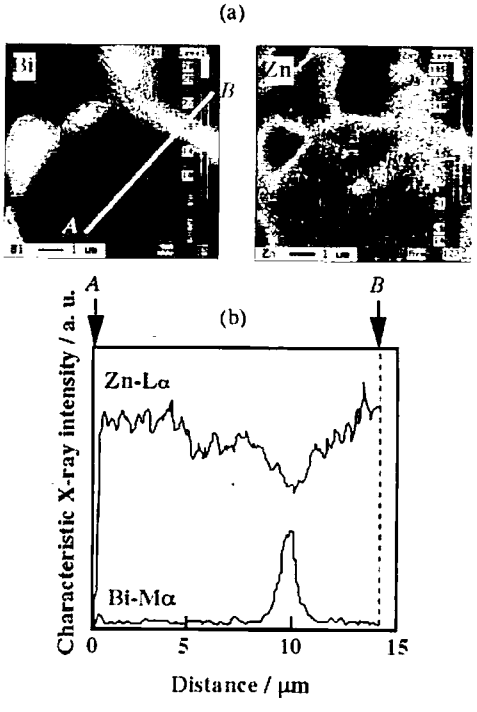

Figure 2.13. EPMA elemental maps (a) of the Bi doped ZnO ceramics and the line analysis (b) from *A* to *B* in the map (a). The doping was carried out at 50 μA at 600 °C for 10 h.

Na and Bi were uniformly doped over the Bi_2O_3 and ZnO ceramics, respectively. Notice that Bi^{3+} easily moves from Bi_2O_3 into the ZnO in the present SOED system. In general, it is well known that the movement of the M^{3+} cation is difficult [9], although Imanaka et al. have found that some M^{3+} cations such as Al^{3+}, Y^{3+} and Sc^{3+} ions move in some tungstates under DC bias (> about 10 days at 900-1000 °C) [14, 15]. In principle, the easy movement of the Bi^{3+} ion in the present SOED system is based on maintaining electrical neutrality by cation movement (Eqs. (1)-(5)) as well as the electron, hole and oxygen anion blocking [16]. Figure 2.13 (a) and (b) show the EPMA elemental distribution maps of the grain boundaries of the Bi-doped ZnO ceramics and the line profile from *A* to *B* shown in the map (a), respectively. This figure indicates that Bi was uniformly distributed over the entire sample on a macro-scale, but it existed as $\gamma\text{-}Bi_2O_3$ in the grain boundaries on a micro-scale, according to an XRD analysis.

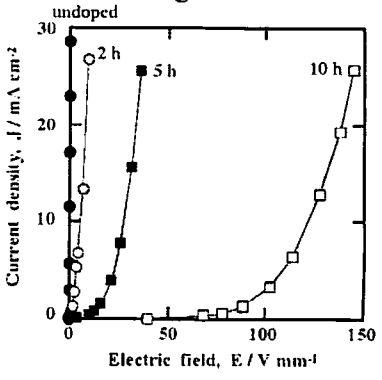

Figure 2.14. Electric field - current density (E-J) characteristics of the ZnO doped with Bi for 2, 5, and 10 h.

Figure 2.14 shows the electric field – current density (E-J) curves at room temperature for ZnO ceramics doped with Bi in the present system. Notice that the curve shifts to a

higher electric field with the increase in the electrolysis time which reflects the increase in the amount of doped Bi. It should also be noticed that the amount of Bi-doped calculated from the electric charge using Faraday's law was about 10^{-2} mol% for the electrolysis for 10 h. This value is very small compared with the case for the conventional method (a few mol%). This is due to the selective doping of the Bi^{3+} only into the grain boundaries of the ZnO ceramics. The selective doping is also one of the important features of the SOED method.

Figure 2.15 shows the breakdown field and nonlinearity coefficient (α) of the sample as the varistor parameters for the present Bi-doped ZnO as a function of the electrolysis time. In general, the breakdown field can be controlled by the grain size of the ZnO ceramics [17-21]. The breakdown field increases with the increase in the number of the grain boundaries containing Bi_2O_3 in the Bi-doped ZnO varistor, because the Bi_2O_3 grain boundaries act as the electrical barrier which then determines the varistor properties. The brakdown field is predicted to be about 10^2 V mm^{-1} for about a 10 μm grain size of the present ZnO ceramics, if all the grain boundaries are doped [22]. This situation will be satisfied for about a 10 h electrolysis using the present Bi-doped ZnO as shown in Fig. 2.15. For cases of an electrolysis time shorter than 10 h, Bi will not be doped into all of the grain boundaries in the ZnO ceramics.

The nonlinearity coefficient was 4-12 for all the samples shown in Fig. 2.15. Although these values are close to those reported for the binary Bi_2O_3-ZnO ceramic varistor prepared by the conventional doping method [23-27], these are not sufficient for a practical application. Therefore, the study of the SOED method for the ternary MO_x-Bi_2O_3-ZnO [26, 27] is still in progress for practical use.

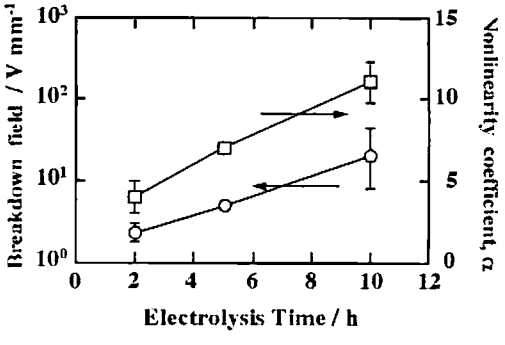

Figure 2.15. Breakdown field and nonlinearity coefficient (α) of the Bi-doped ZnO ceramics as a function of the electrolysis time.

Consequently, it should be noted that Bi^{3+}, which is considered difficult to move, is easily transported by the present SOED method. Moreover, it was found that the properties of the ZnO varistor can be easily controlled by the electric charge during the electrolysis of selective Bi-doping into the grain boundaries. The success of the Bi doping using the system show in Fig. 2.12 suggests that all of the cations constituting the oxides or salts such as Bi_2O_3 can be doped into functional ceramics.

2. 5. Electrosubstitution at the metal, metal compounds / Na-β"-Al_2O_3 interface

The anode M is the source of the doping cation M in the SOED method, and the M cation drifts through the M-β"-Al_2O_3 solid electrolyte, as shown in Fig. 2.16(a). Therefore, Ag metal together with Ag- β"-Al_2O_3 has been used as the anode when the dopant was Ag. Moreover, Ag metal has been used as the anode even when the dopant was the cation other than Ag, where Ag is not M in the M- β"-Al_2O_3. This condition is satisfied when the amount of the needed dopant M was small and the Ag^+ ion did not affect the functional properties of the oxide ceramics, because the electrochemical reaction from Ag to Ag^+ always occurs at the Ag / M-β"-Al_2O_3 interface and trace amounts of Ag^+ were doped into the oxide ceramics as well as the dopant M during the electrolysis. The same metal M as the M cation in the M-β"-Al_2O_3 must be used as the anode if a relatively large amount of pure M cation needs to be doped into the oxide ceramics. However, the use of a metal as

the anode will be difficult when the dopant is an alkaline, alkaline earth, or lanthanide cation. In this

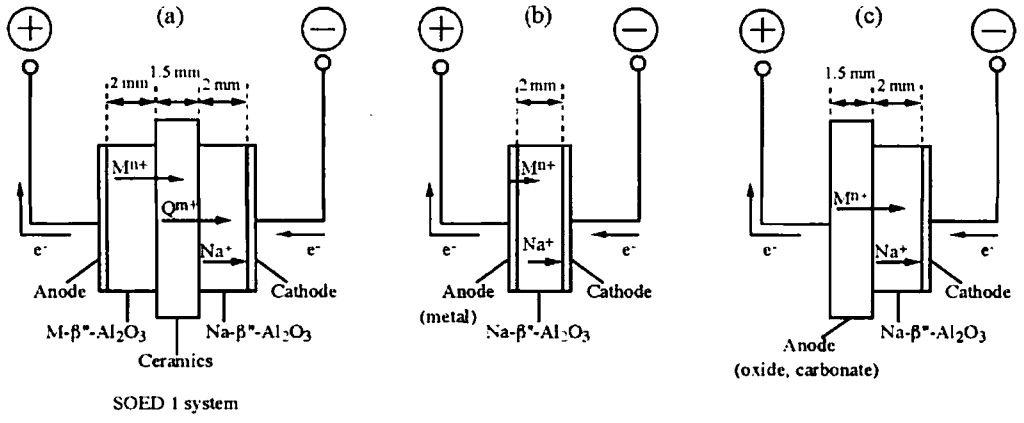

Figure 2.16. Electrosubstitution system. (a) SOED 1 system, where Na+ in the Na-β"-Al_2O_3 is substituted for the Q^{m+} cation pushed by the injection of the M^{n+} cation. (b) Electrolysis system, where metal cation from pure metal is electrosubsituted for Na in Na-β"-Al_2O_3. (c) Direct injection system, where M^{n+} is directly substituted for Na+.

case, a metal salt such as carbonate or oxide may be useful as the anode.

In this section, some metal carbonates, metal oxides as well as some pure metals were used as the anode, and their electrochemical reactions and electro-substitutions have been studied at the Na-β"-Al_2O_3 interface.

2. 5. 1. Experimental

In the present experiment, Ag and Pt plates (thickness: 0.3 mm for Ag, 0.1 mm for Pt) were used as the metal anode. On the other hand, some carbonates (K2CO3, SrCO3) and metallic oxides (TiO_2, Fe_2O_3, CuO, $YBa_2Cu_3O_y$ (YBCO), $La_{0.8}Sr_{0.2}MnO_3$ (LSMO), $Bi_2Sr_2CaCu_2O_y$ (BSCCO)) were used as the compound anode. The pellet samples of the carbonates and oxides (ceramics in (a) and anode in (c) in Fig. 2.16, thickness: 1.5 mm, surface area: 0.8 cm^2) were prepared by pressing the powder at 1000 kg/cm^2 and heating at 800-1250 °C. Na-β"-Al_2O_3 (Nihon Tokushu Togyo Co., Ltd., thickness: 2 mm) was used as the solid electrolyte and a Pt plate was used as the cathode. The electrochemical doping was carried out under a constant current density at 400-800 °C in air using the experimental setup schematically shown in Fig. 2.16. The appropriate doping temperatures where no thermal diffusion occurred but rather electro-substitution at the interfaces of the metal, metal compounds / Na- β"-Al_2O_3, were selected for all the electro-substitution tests. The apparent contact area in the anode / Na-β"-Al_2O_3 was 0.10-0.19 cm^2. After the electrolysis, the distribution state of the dopants in a cross section of the Na-β"-Al_2O_3 was analyzed using electron probe microanalysis (EPMA).

2. 5. 2. Results and discussion

Metal / Na-β"-Al_2O_3 interface ((b) in Fig. 2.16)

The following reactions for the electro-substitution occur at the metal anode / Na-β"-Al_2O_3 and Na-β"-Al_2O_3 / cathode interfaces in Fig. 2.16 (b).

$M \rightarrow M^{n+}$ (Na-β"-Al_2O_3) + ne^- (anode) (1)

Na^+ (Na-β"-Al_2O_3) + $e^- \rightarrow Na$

$2Na + CO_2$ (in air) + $(1/2)O_2 \rightarrow Na_2CO_3$ (cathode) (2)

The production of Na_2CO_3 at the Na-β"-Al_2O_3 / Pt (cathode) interface was detected by the X-ray analysis. However, no reaction occurred when Pt was used as the anode.

The Ag electro-substitution for Na easily occurred when using the Ag anode. The following reaction occurs at the Ag / Na-β"-Al_2O_3 interface.

$$Ag \rightarrow Ag^+ (Na\text{-}\beta''\text{-}Al_2O_3) + e^- \quad (3)$$

Figure 2.17 shows the atomic ratios of Ag / Al and Na / Al in the Ag substituted Na-β"-Al_2O_3 as function of the distance from the Ag / Na-β"-Al_2O_3 interface which were analyzed by the EPMA. The amount of the substituted Ag is relatively large on the side of the Ag / Na-β"-Al_2O_3 interface, while that of Na is relatively small on the same side. Thus, the present electro-substitution produces the concentration gradient of the substituted Ag in the Na-β"-Al_2O_3. All the current efficiencies of the Ag electro-substitution calculated from Eq. (3) and Faraday's law, approximately were 100 %. This is due to the electro-substitution but not the thermal diffusion, because no doping occurred under no bias. Thus, the electro-substitution of Ag for Na in the Na-β"-Al_2O_3 was relatively easy, and demonstrates its utility as the anode source in the SOED method.

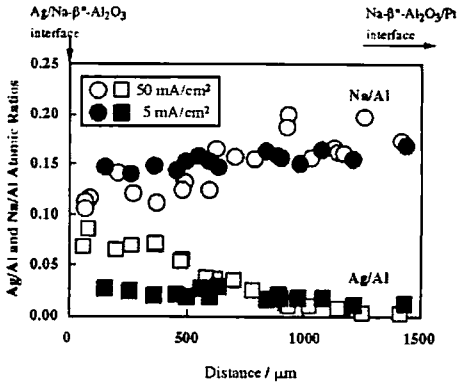

Figure 2.17. Atomic ratios Ag/Al and Na/Al in the Ag substituted Na-β"-Al_2O_3 at 400 °C as a function of the distance from the Ag/ Na-β"-Al_2O_3 interface.

Metal compounds / Na-β"-Al_2O_3 interface ((c) in Fig. 1)

The following decomposition reaction probably proceeds at the alkaline metal carbonate anode / Na-β"-Al_2O_3 interface in the Fig. 2.16(c) system.

$$M_2CO_3 \rightarrow 2M^+ (Na\text{-}\beta''\text{-}Al_2O_3) + CO_2 + (1/2)O_2 + 2e^- \quad \text{(alkaline metal carbonate anode)} \quad (4)$$

Figure 2.18 shows the applied voltages for the K_2CO_3 / Na-β"-Al_2O_3 at 400 °C and $SrCO_3$ / Na-β"-Al_2O_3 interfaces at 750 °C as a function of the electrolysis time. The applied voltage was very large for the latter case, suggesting that the Sr electro-substitution is relatively difficult. In fact, no substitution occurred at 400 °C for this case, but did occur at 750 °C. Figure 2.19 shows the atomic ratios of K/Al and Na/Al in the K substituted Na-β"-Al_2O_3 at 400 °C as a function of the distance from the K_2CO_3 / Na-β"-Al_2O_3 interface which was analyzed by EPMA. The graded substitution, which is similar to the case of the Ag / Na-β"-Al_2O_3 (Fig. 2.17), occurred again as shown in Fig. 2.19.The current efficiencies for the Sr and K electro-substitutions calculated from Eq. (4) and Faraday's law, were about 100 %. These are again due to the electro-substitution but not the chemical diffusion, because no doping occurred under no bias at the above temperatures, although the chemical diffusion of K^+ ions from K_2CO_3 to Na-β"-

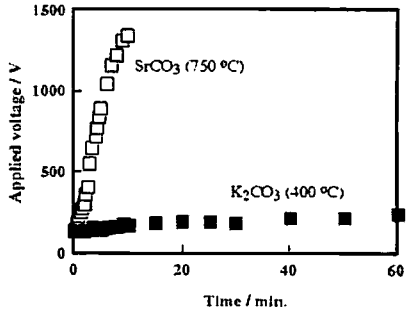

Figure 2.18. Applied Voltages as a function of the electrolysis time for the K_2CO_3 / Na-β"-Al_2O_3 and $SrCO_3$ / Na-β"-Al_2O_3 for a constant current density of 5 mA/cm² in the system in Fig. 2.16(c).

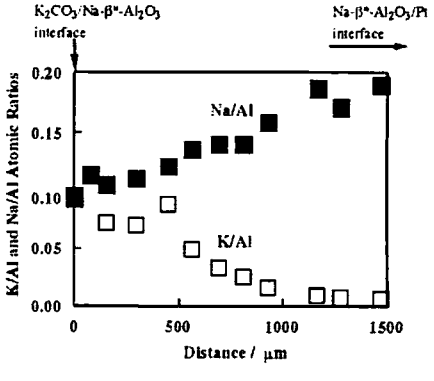

Figure 2.19. Atomic ratios K/Al and Na/Al in the K substituted Na-β"-Al_2O_3 for constant current of 5 mA/cm² at 400 °C after 60 min electrolysis as a function of the distance from the K_2CO_3 / Na-β"-Al_2O_3 interface.

Al_2O_3 was observed under no bias at 750 °C according to the EPMA analysis. In conclusion, some metal carbonates can act as the anode source material for the electrosubstitution.

Some oxides were also tested as the anode for the electro-substitution in Fig. 2.16(c) system. In this case, the following reaction will occur at the oxide anode.

$$MO_n \rightarrow xM^{m+}(Na\text{-}\beta''\text{-}Al_2O_3) + xme^- + M_{1-x}O_n \quad (5)$$

The reaction (5) will be followed by the decomposition reaction (6), if the cation vacancy, *m*, is large.

$$M_{1-m}O_n \rightarrow M_{1-m}O_{n-m} + (m/2)O_2 \quad (6)$$

To dope with Cu or Fe, CuO or Fe_2O_3 anodes were used, but no doping (< 0.1 atm%) occurred for the these electrode even at 800 °C. The complex oxides such as YBCO, LSMO, and BSCCO were also tested as anodes. Ba or Sr were mainly doped by using the YBCO or BSCCO and LSMO, respectively. However, their current efficiencies were less than 10 %. Thus, the electro-substitution using an oxide anode was difficult. Consequently, the oxide may not be suitable as an anode material.

There will be two important factors, which affect the electro-substitution process. One is the cation migration in the Na-β"-Al_2O_3 which occurs after the electrochemical reaction at the anode / Na-β"-Al_2O_3 interface. Ag^+ and K^+ have a higher conductivity compared to the other cations in β"-Al_2O_3 [5, 13]. As a result, the electrosubstitution is easier for these cations. On the other hand, the electro-substitution by Pt or Ti does not occur, because these metals do not readily transport in the Na-β"-Al_2O_3. The other important factor is the activation energy necessary for the decomposition represented by Eqs. (4) and (6). In general, metal carbonates more easily decompose compared with oxides. Therefore, some metal carbonates will satisfactorily act as the anode, but not oxides as already stated.

2. 6. Conclusions

In this chapter, we have examined the cation doping by using the SOED 1 system and clarified the doping mechanism. In general, the SOED 1 method is very useful for the doping into only grain boundaries of oxide ceramics using a selective cation, if the doping is carried out under low current or low voltage. Moreover, significant cation doping into the bulk will sometimes occur for the Ca doping into YBCO or Zn doping into BSCCO ceramics under high current density, which will simultaneously reflect the degree of the bond strength of the constituting cation in the structure. In addition, the new type of the SOED 1 system was proposed, and the trivalent Bi^{3+} doping into ZnO ceramics was achieved. Bi-doped ZnO ceramics showed a performance as a varistor and its property was simply controlled by the doping time. Finally, the anodic reaction at the metal or metal compounds / Na-β"-Al_2O_3 interface was investigated. Since metal cation eliminated from M or MCO_3 was injected into β"- Al_2O_3 structure, we could demonstrate that some metals and metal carbonates are valuable as anode in the SOED method.

2. 7. References

[1] Y. Matsumoto, J. Hombo, Y. Yamaguchi, M. Nishida, A. Chiba, *Appl. Phys. Lett.* **56**, 1585 (1990).

[2] Y. Matsumoto, Y. Yamaguchi, J. Hombo, T. Hauber, W. Gopel, *J. Solid State Chem.* **98**, 201

(1992).
[3] Y. Matsumoto, K. Funaki, J. Hombo, Y. Ogawa, *J. Solid State Chem.* **99**, 336 (1992).
[4] M.S. Whittingham, R.A. Huggins, *J. Electrochem. Soc.* **118**, 1 (1971).
[5] G.C. Farrington, B. Dunn, *Solid State Ionics* 7, 267 (1982).
[6] M. Breiter, M.M. Schreiber, B. Dunn, *Solid State Ionics* **18-19**, 658 (1986).
[7] Y. Zhao, H. Zhang, S. Sun, M. Zhang, Z. Chen, Q. Zhang, *Physica C* **153-155**, 1665 (1988).
[8] M. Fujiwara, M. Nagae, Y. Kusano, T. Fujii, J. Takada, *Physica C* **274**, 317 (1988).
[9] K. Hoshino, N.L. Peterson, *J. Phys. Chem. Solids* **8-9**, 963 (1984).
[10] B. Dunn, G.C. Farrington, *Solid State Ionics* **9-10**, 223 (1983).
[11] J. Köhler, N. Imanaka, W. Urland, G. Adachi, *Angew. Chem. Int. Ed.* **39** 904 (2000).
[12] M.S. Whittingham, R.A. Huggins, *J. Chem. Phys.* **54**, 414 (1971).
[13] J.L. Briant, G.C. Farrington, *J. Solid State Chem.* **33**, 385 (1980).
[14] N. Imanaka, Y. Kobayashi, K. Fujikawa, K. Asano, Y. Okazaki, G. Adachi, *Chem. Mater.* **10**, 2006 (1998).
[15] Y. Kobayashi, T. Egawa, Y. Okazaki, S. Tamura, N. Imanaka, G. Adachi, *Solid State Ionics* **111**, 59 (1983).
[16] Y. Matsumoto, *Solid State Ionics* **100**, 165 (1997).
[17] D.F.K. Hennings, R. Hartung, P.J.L. Reijnen, *J. Am. Ceram. Soc.* **73**, 645 (1990).
[18] T. Asokan, R. Freer, *J. Mater. Sci. Lett.* **13**, 925 (1994).
[19] G. Agarwal, R.F. Speyer, *J. Mater. Res.* **12**, 2447 (1997).
[20] A.I. Ivon, A.B. Glot, A.V. Gaponov, S.V. Mazuriku, *Key Eng. Mater.* **132-136**, 1289 (1997).
[21] E. Olsson, G. Dunlop, R. Osterlund, *J. Am. Ceram. Soc.* **76**, 65 (1993).
[22] T.K. Gupta, *J. Am. Ceram. Soc.* **73**, 1817 (1990).
[23] J. Wong, *J. Appl. Phys.* **51**, 4453 (1980).
[24] Y. Shim, J.F. Cordaro, *J. Am. Ceram. Soc.* **71**, 184 (1988).
[25] S. Tanaka, C. Akita, N. Ohashi, J. Kawai, H. Haneda, J. Tanaka, *J. Solid State Chem.* **105**, 36 (1993).
[26] M. Matsuoka, *Jpn. J. Appl. Phys.* **19**, 736 (1971).
[27] A. Smith, D.S. Smith, P. Abelard, *Mater. Lett.* **19**, 159 (1994).

Chapter 3

Mechanism of Cation Doping by the SOED 2 Method

3.1.Introduction

Electrochemical cation doping (M^{n+}) into oxide ceramics at relatively low temperature (400 - 600 °C) was investigated using the SOED 1 system (anode / M-β"-Al_2O_3 / Oxide Ceramics / M-β"-Al_2O_3 / cathode) in chapter 2, [1-4] where a M^{n+} conductor blocks electron and oxide ion migration in the system. The SOED 1 method is very useful for the doping into only grain boundaries of oxide ceramics using a selective cation, if the doping is carried out under low current or low voltage. Moreover, significant cation doping into the bulk will sometimes occur for other oxide ceramics using the SOED 1 method [2, 5]. On the other hand, the SOED 2 method is one of main system in the present technique, where metal cation and oxide ion are simultaneously injected into the target materials [6]. Therefore, the purpose in this section is to evaluate the SOED 2 system for cation doping into three kinds of oxide ceramics with different conductive properties, and to draw a distinction of the characteristics between the SOED 1 and 2.

3. 2. Experimental

Experiments were carried out using oxides including the superconductor $YBa_2Cu_3O_y$ (YBCO, Dowa Kogyo Co.), the semiconductor Fe_2O_3 (Nacalai Tesque Co.) and the insulator $BaTiO_3$ (Fuji Titanium Co.) as the doping target. The sintered pellet samples (thickness: 1.5 mm, surface area: 0.6 cm^2) of each of these oxides were prepared by pressing the powders under 1000 kg/cm^2 and heating at 930 - 1300 °C. The cation conductors, M-β"-Al_2O_3 (M = Na, Ag, Sr, and Ca), were prepared by substitution of M for Na in Na-β"-Al_2O_3, where the Na-β"-Al_2O_3 (Nihon Tokushu Togyo Co.)

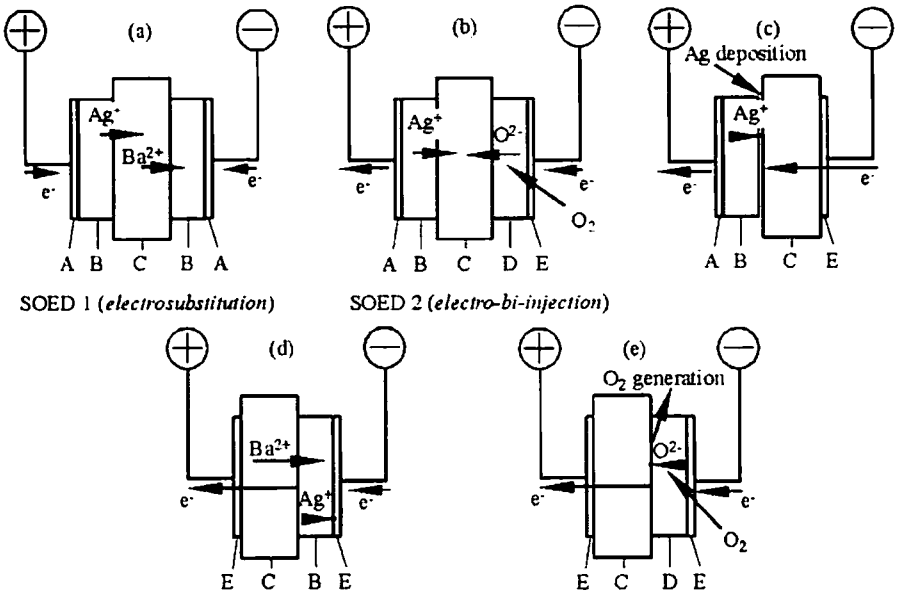

Figure 3.1. Models of the ion migration for various SOED methods. A, Ag; B, Ag-β"-Al_2O_3; C, ceramics; D, YSZ; E, Pt.

polycrystal pellet was immersed in the appropriate molten salt consisting of M as previously noted [6-8]. Y-stabilized ZrO_2 (YSZ, 8 mol%Y_2O_3-ZrO_2, Nikkato Co.) was used as an oxide ion conductor in the SOED 2 system. The apparent contact area in the M-β"-Al_2O_3/ceramics was 0.2 cm^2. The good contact in the ceramic/ceramic interfaces which avoids the current inhomogeneities, has been achieved by rubbing the ceramics strongly each other. The electrolysis was carried out for three hours under a constant current density at 400 or 600 °C. No cation doping occurred in the absence of bias at these temperatures. After the electrolysis, the elemental distribution of the dopant in a cross section of the doped ceramics was measured using electron probe microanalysis (EPMA). The crystal structure of the samples was analyzed from the X-ray diffraction (XRD) patterns.

3. 3. Results and discussion

The basic migration mechanism in the present SOED 2 system for the Ag^+ doping into YBCO is illustrated in Fig. 3.1 (b). Ag is electrochemically oxidized to Ag^+ at the interface of Ag/Ag-β"-Al_2O_3, and then Ag^+ in the Ag-β"-Al_2O_3 is injected into the oxide ceramics. Oxygen in the air is electrochemically reduced to O^{2-} at the YSZ/Pt interface, and O^{2-} is injected into the oxide ceramics. Therefore, this doping scheme corresponds to "electro-bi-injection". The following overall reaction in the SOED 2 system will occur in the ceramics together with the electrochemical reactions at the anode (oxidation of metal into cation) and cathode (O_2 reduction into O^{2-}):

$$2M^{n+}\ (M\text{-}\beta\text{''-}Al_2O_3) + nO^{2-}\ (YSZ) + \text{ceramics} \rightarrow M_2\text{-}O_n\ (\text{ceramics})$$

Experimental results for the doping with various cations by the SOED 2 system are listed in Table 3.1. Two doping types, A and B, are represented in this table. Type A corresponds to a graded doping at the anode side of the ceramic sample while type B corresponds to uniform doping over the entire ceramic sample. A third type (type C) corresponds to no doping but metal or oxide was

Table 3.1. Experimental results in the SOED 2 method.

Ceramics	Current density (mA/cm^2)	Doping cation	Electrolysis temperature (°C)	a), b) Doping type
$YBa_2Cu_3O_y$	5	Ag^+	400	A
			600	A
	0.5	Na^+	400	B
			600	B
	0.5	Sr^{2+}	400	C
			600	A
	0.5	Ca^{2+}	400	C
			600	A
$BaTiO_3$	0.5	Ag^+	400	C
			600	A
	0.5	Sr^{2+}	400	C
			600	A
Fe_2O_3	0.5	Ag^+	400	A
			600	A
	0.5	Sr^{2+}	400	C
			600	A

a) Main doping point of the all dopants is the grain boundaries in the ceramics.

b) Doping types A, B and C correspond to the graded doping at the anode side of the ceramics, doping over the entire sample and metal or oxide deposition at the anode side interface of M-β"-Al_2O_3/ceramics, respectively.

deposited at the anode side interface of the M-β"-Al_2O_3 / ceramics. The results in this table indicate that various cations can be doped into the oxide ceramics at high temperature and that facile doping is observed for monovalent cations (Ag^+, Na^+) compared with the divalent cations (Sr^{2+}, Ca^{2+}), because monovalent cations were doped at relative low temperature as listed in Table 3.1. These results demonstrate that the SOED 2 system is very useful for the doping into all of the oxide ceramics, i.e., YBCO, $BaTiO_3$ and Fe_2O_3, independent of their conductive properties, but dependent on the electrolysis temperature.

Figure 3.2 shows typical EPMA distribution line scans of the elements in a cross section of the YBCO sample doped with Ag^+ under 5 mA/cm^2 at 600 °C using the SOED 2 system. The Ag dopant was distributed on the anode side of the YBCO ceramics (type A doping). Thus, the graded doping was a general characteristic of the SOED 2 system. Ag was uniformly doped over the entire YBCO sample when the doping was carried out using the SOED 1 system under the same electrolysis condition as previously reported in chapter 2 [1]. In this case, only Ba was detected in the cathode side Ag-β"-Al_2O_3 according to the EPMA analysis. This indicates that only Ba^{2+} ion is released from the YBCO ceramics under an electrical force so that the electrical neutrality is maintained in the ceramics as shown in Fig. 3.1 (a). On the other hand, no Ag doping into the YBCO occurred but Ag metal was deposited at the Ag-β"-Al_2O_3 / YBCO interface, when the system (c) in Fig. 3.1 was used. The oxide ion will not be doped into the YBCO using the electrolysis system (e) but O_2 will be generated at the YBCO/YSZ interface (see (e)) as stated below. From these results, it was judged that the electrochemical cation doping did not occur when electrical neutrality was not maintained in the ceramics. Thus, the injection of the oxide ion is very important for the cation doping in the SOED 2 system.

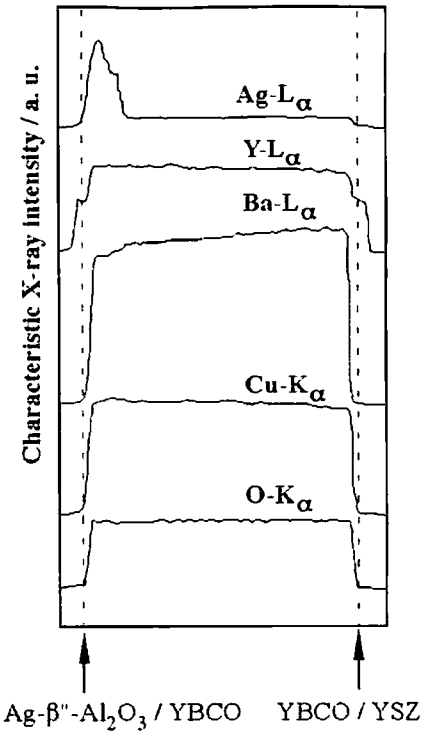

Figure 3.2. EPMA elemental distribution line scans in the cross section of the YBCO doped with an Ag sample at 600 °C by the SOED 2 system.

Figure 3.3 shows the dependence of the applied voltage on the electrolysis time for a constant current density (5 mA/cm^2) at 600 °C. (a), (b), (c), (d) and (e) in this figure correspond to the

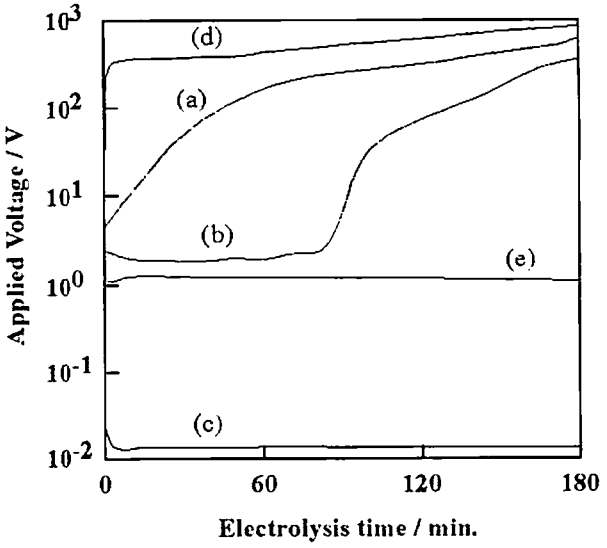

Figure 3.3. Dependence of the applied voltage on the electrolysis time under 5 mA/cm^2. (a)-(e) corresponds to those for the electrolysis systems given in Fig. 3.1, respectively.

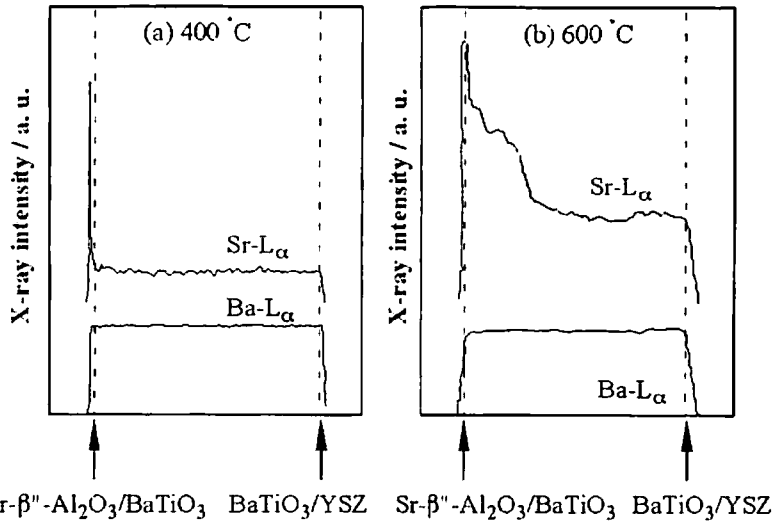

Figure 3.4. EPMA elemental line scans for the $BaTiO_3$ ceramics doped with Sr by the SOED 2 system.

electrolysis systems shown in (a), (b), (c), (d) and (e) in Fig. 3.1, respectively. The applied voltage in (b) was lower than that in (a) during the initial stage of the electrolysis, but abruptly increased with the electrolysis time at 90 min. In the SOED 1 system (a), a large voltage will be mainly based on the applied voltage for the Ba^{2+} migration through the YBCO ceramics. The large applied voltage for the electrolysis system (d) indicates that the direct injection of Ba^{2+} from the YBCO into Ag-β"-Al_2O_3 is difficult. For the electrolysis systems (c) and (e), their applied voltages were small compared with those of the other systems, and were close to the voltages calculated from both ionic conductivities of Ag^+ and O^{2-} in Ag-β"-Al_2O_3 and YSZ, respectively. This indicates that no doping of these ions into the YBCO ceramics occurs. Consequently, the following phenomena will occur in the SOED 2 system. Initially, both Ag^+ and O^{2-} ions are smoothly injected into the YBCO ceramics until the amount of the Ag^+ doped into the anode side of the YBCO saturates (< 90 min in (b)). The applied voltage is not so large in this stage. After the saturation, the Ag^+ will be difficult to migrate in the ceramics where the applied voltage increases with the electrolysis time (> 90 min in (b)). In fact, both distribution states of the Ag dopant (graded doping) after 90 and 180 min electrolysis were similar to each other, according to the EPMA analysis.

An X-ray qualitative analysis was carried out in some sections of the YBCO sample doped with Ag at 600 °C by the SOED 2 system. Two micropoints were analyzed in the cross section of the doped sample. One is the area analysis which corresponds to all parts of the doped sample, i.e., grain bulk and grain boundaries in the sample. The other is a pinpoint analysis to detect the elements only in the grain bulk. The peak attributed to Ag was observed only in the area analysis. This indicates that Ag was selectively doped only in the grain boundaries. Thus, both Ag and oxygen migrate more smoothly in the grain boundaries than in the bulk. Other cations such as Na^+, Sr^{2+} and Ca^{2+} were also doped into the grain boundaries. Thus, the SOED 2 method is very useful for selective doping in the grain boundaries.

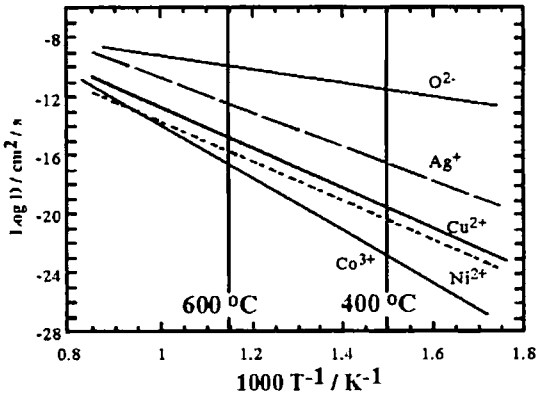

Figure 3.5. Arrhenius plots of oxide ion and metal cations in YBCO ceramics [9-12].

Composition and lattice parameters of both contact surfaces in the Ag-doped YBCO sample prepared by the SOED 2 system were

analyzed from XRD patterns. Only a small amount of impurities such as $BaCO_3$, CuO and Ag metal were detected on the anode side surface, while no change was observed on the cathode side surface. In principle, the cation doping using the SOED 2 system will proceed without any destruction of the crystal, since the doping occurs only in the grain boundaries without cation exchange. In fact, no change in the lattice parameters of the doped YBCO was observed. Therefore, the SOED 2 system may be more useful than the SOED 1 system (electrosubstitution), when the substitution of the dopant cation is difficult in the ceramics.

The electrolysis temperature is very important for the doping using the SOED 2 system. Figure 3.4 shows two EPMA distribution line scans of the elements in the Sr-doped $BaTiO_3$ ceramics under 0.5 mA/cm^2 at 400 °C and 600 °C. Sr was not doped into the $BaTiO_3$ but deposited at the β"-Al_2O_3 / $BaTiO_3$ anode interface as SrO at 400 °C. On the other hand, Sr was doped into the $BaTiO_3$ ceramics at 600 °C as the figure shows (graded doping). The same phenomena were also observed for the cases of the Sr and Ca-doping into the YBCO, the Ag-doping into the $BaTiO_3$ and the Sr-doping into the Fe_2O_3, as listed in Table 3.1. In these cases, Ag, Sr and Ca were deposited as a metal or oxide at the anode side interfaces at 400 °C analogous to Fig. 3.4 (400 °C). In the SOED 2 system, the doping will be determined by the degree of the migration rates of the cation dopant and the oxygen anion in the grain boundaries. Figure 3.5. shows the Arrhenius plots of the self-diffusion coefficient of oxide ion and metal cations in YBCO structure [9-12]. It is well-known that the diffusion rate of the oxygen anion through the oxide ceramics is much larger than that of the metal cation. Therefore, cation doping will be generally difficult at low temperature. Both migration rates of the cation dopant and the oxygen anion will come close each other at high temperature, because the activation energy of the cation diffusion through the oxide ceramics is larger than that of the oxygen anion. For example, activation energies of the Ag^+ and oxygen anion diffusion through the YBCO ceramics are 2.2 and 1.5 eV, respectively [10, 13]. Consequently, the cation doping into the oxide ceramics occurs easily at relatively high temperatures for the SOED 2 system.

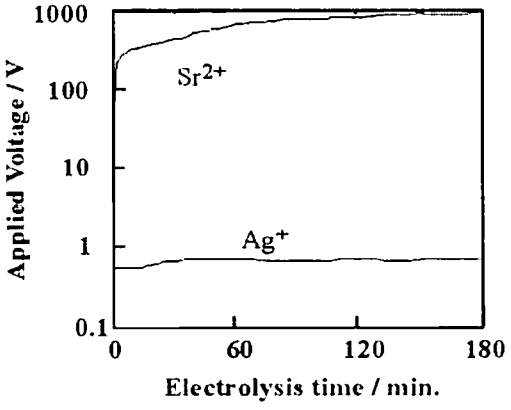

Figure 3.6. Dependency of the applied voltage on the electrolysis time under 0.5mA/cm² at 600 °C in SOED 2 system.

The doping by the SOED 2 system also depends on the valence of the dopant cation as already stated. For the Ag and Sr-doping into the Fe_2O_3, the monovalent cation (Ag^+) can be easily doped into the Fe_2O_3 at both 400 and 600 °C, while the divalent cation (Sr^{2+}) can be doped at 600 °C but not at 400 °C (Table 3.1). Figure 3.6 shows the dependence of the applied voltage on the electrolysis time under 0.5 mA/cm^2 for the Ag and Sr doping into the Fe_2O_3 at 600 °C. The applied voltage can somewhat reflect the degree of the migration rate, and will be small when the migration rate is large. The applied voltage for the case of Sr^{2+} was about three orders of magnitude larger than that for the case of Ag^+, and reached about 10^3 V after 180 min. In general, the ionic conductivity of the metal cation in the oxide ceramics depends on its valence. For example, the ionic conductivity of the monovalent cation in the M-β"-Al_2O_3 is higher than that of the divalent one, because the divalent cation is more significantly affected than the monovalent cation by electrostatic interaction from the oxygen lattice of the spinel structure in the M-β"-Al_2O_3. The Na doping into the YBCO is very easy compared with the case of the Ag doping, since the former doping corresponds to type B but the latter corresponds to type A (Table 3.1). This difference can also be explained from the degree in the migration rate. The ionic

conductivity is higher for Na^+ than Ag^+ in the M-β"-Al_2O_3 [14], although it seems to depend on the structure of the oxide ceramics to be doped.

The SOED 2 system gave an important possibility of the preparation for the graded materials in application. The graded state of the dopant can be easily controlled by the electrolysis temperature, electrolysis time, and electrolysis current density. For example, an improvement of some thermoelectric materials can be achieved by the graded doping using the SOED 2 method.

3. 4. Conclusions

Electrochemical cation doping into various oxide ceramics together with the injection of the oxygen anion was carried out using the SOED 2 method. The following important information was obtained and a doping mechanism was proposed.

1. The cation doping easily occurred together with the oxide ion injection so that electrical neutrality was maintained in the ceramics.
2. Various cations were easily doped into the grain boundaries of the oxide ceramics at relatively high temperature. This will be based on the higher activation energy for the cation migration than for the oxygen anion migration in the grain boundaries of the oxide ceramics.
3. The graded doping at the anode side of the oxide ceramics generally occurred for the SOED 2 system. This will be based on the faster migration for the oxide ion than for the dopant cation.
4. The doping was easier for the monovalent cation than for the divalent cation. This tendency was in harmony with the degree of the cation migration rate in the M-β"-Al_2O_3.

3. 5. References

[1] Y. Matsumoto, M. Koinuma, H. Yamamoto, T. Nishimori, *Solid State Ionics* **95**, 309 (1997).

[2] Y. Matsumoto, T. Nishimori, H. Yamamoto, K. Nishimura, K. Kamada, A. Ogata, *Solid State Ionics* **107**, 41 (1998).

[3] Y. Matsumoto, *J. Solid State Chem.* **128**, 93 (1997).

[4] Y. Matsumoto, *Solid State Ionics* **100**, 165 (1997).

[5] K. Kamada, Y. Yanaru, Y. Matsumoto, *Electrochemistry* **68**, 540 (2000).

[6] M.S. Whittingham, R.A. Huggins, *J. Electrochem. Soc.* **118**, 1 (1971).

[7] M. Breiter, M.M. Schreiber, B. Dunn, *Solid State Ionics* **18-19**, 658 (1986).

[8] G.C. Farrington, B. Dunn, *Solid State Ionics* 7, 263 (1982).

[9] S.J. Rothman, J.L. Routbort, *Phys. Rev.* **B44**, 2326 (1991).

[10] N. Chen, S.J. Rothman, J.L. Routbort, *J. Appl. Phys.* **68**, 2523 (1990).

[11] J.L. Routbort, S.J. Rothman, N. Chen, J.N. Mundy, *Phys. Rev.* **B43**, 5489 (1991).

[12] D. Gupta, R.B. Laibowitz, J.A. Lacey, *Phys. Rev. Lett.* **64**, 2675 (1990).

[13] D.J. Vischjager, P.J. Van Der Put, J. Schram, J. Schoonman, *Solid State Ionics* **27**, 199 (1988).

[14] J.L. Briant, G.C. Farrington, *J. Solid State Chem.* **33**, 385 (1980).

Chapter 4

Pinpoint Doping Using a β"-Al_2O_3 Microelectrode

4. 1. Introduction

Ion conducting microcontacts (microelectrodes) have been widely used in the research field on *solid state ionics*. Concretely, microelectrodes play a significant role in the measurements of local conductivities in ceramic materials [1], transference numbers in mixed conductors [2, 3], and in the determination of redox potentials in metal oxides [4, 5]. The use of a microelectrode allows a better control of electrochemical parameters and contact areas at the interface compared to a conventional planar electrode, which often shows time-dependent changes of the contact area because of its inhomogeneous interface [6, 7].

The SOED method will be very useful for pinpoint doping into the desired position of samples if the contact area between β"-Al_2O_3 and the doping target remains small during the electrolysis. In this chapter, the pinpoint cation doping into a selected area of the doping target has been carried out using a M-β"-Al_2O_3 microelectrode to develop a new field of applications of the SOED method. In our knowledge, ion conducting microelectrodes have never been applied to a doping study. This section reports in detail the relationship between the distribution state of the dopant and the conditions of pinpoint doping using the SOED method.

4. 2. Experimental

Electrochemical pinpoint doping was carried out using the two types of experimental setup shown in Fig. 4.1, where the M-β"-Al_2O_3 and Y-stabilized zirconia (YSZ) were used as a cation and oxide ion conductor. A M-β"-Al_2O_3 (M = Ag, Li, K, Pb, Sr and Ca) microelectrode was prepared by the substitution of M for Na in Na-β"-Al_2O_3. A Na-β"-Al_2O_3 polycrystalline pellet (Nihon Tokusyu Togyo Co.; thickness: 2 mm, diameter: 7 mm) was immersed in molten salts at an appropriate temperature [8-10]. That the Na was completely exchanged, it was confirmed by an electron probe micro analysis (EPMA) in the cross section of β"-Al_2O_3. The obtained M-β"-Al_2O_3 was polished

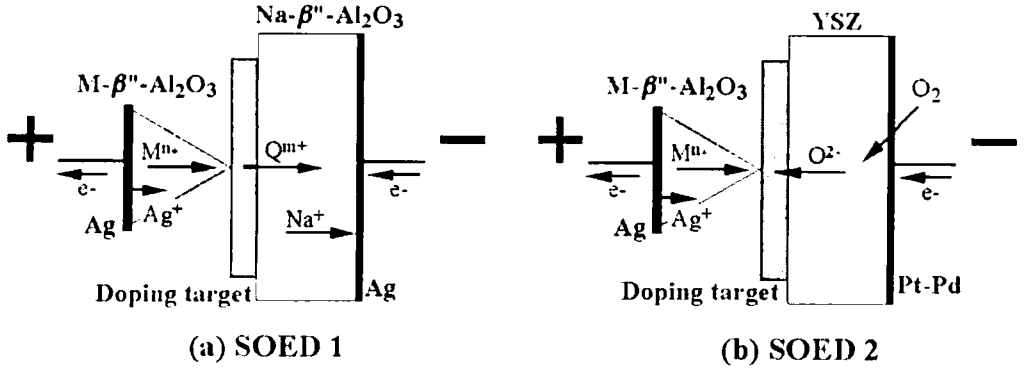

Figure 4.1. Models of ion migration for the pinpoint doping by the SOED method, where (a) and (b) show the SOED 1 "electrosubstitution" SOED 2 "electro-bi-injection" mechanism, respectively.

with emery paper to form a quadrangular pyramid-like microelectrode as shown in Fig. 4.2. Assuming a hemispherical microcontact between M-β"-Al_2O_3 and a doping target, a typical value of the contact radius was about 10 μm. A borosilicate glass plate (Matsunami Glass Ind.; thickness: 0.15 mm) and $Bi_2Sr_2CaCu_2O_y$ ceramics (BSCCO, Dowa Kogyo Co. Ltd.; thickness: 0.7 mm) were used as doping targets. Cation doping was performed at a constant current with a regulated DC power supply at 300 – 600 °C in air. No doping occurred in the absence of the electric field. After doping, the distribution state of the dopant in the anodic surface and the cross section of the doping target was analyzed by EPMA. The crystal structure of a doped sample was also analyzed by X-ray diffraction (XRD) measurements.

Figure 4.2. Typical SEM image of the top of a β"-Al_2O_3 microelectrode.

4. 3. Results and discussion

Figure 4.1 illustrates the basic cation migration mechanism in the present SOED system for pinpoint doping, where two different electrolysis systems were employed (SOED 1 and 2). Na-β"-Al_2O_3 and YSZ are used at the cathodic side interface in the SOED 1 (a) and SOED 2 (b), respectively.

Figure 4.3 shows typical EPMA elemental distribution maps of the anodic surface of pinpoint Ag-doped alkali borosilicate glass using SOED 1 system. Ag was distributed in the manner of a circle drawn with its center at the Ag-β"-Al_2O_3 / glass microcontact. The characteristic X-ray intensity of Na decreased at the area where silver was detected. Na was detected in the cathode side β"-Al_2O_3 when Ag-β"-Al_2O_3 was used instead of Na-β"-Al_2O_3. These results indicate that Ag^+ is electrochemically substituted for Na^+ in the glass and that the cation migrations as illustrated in Fig. 4.1(b) proceeded during the electrolysis. The SOED 2, however will be not suitable for doping into the glass since oxide ion conductivity in the glass is extremely small.

The diameter of the Ag-doped area on the anodic surface strongly depended on the applied electric charge which reflects the amount of Ag doping. That is, the Ag distribution diameter increased with increasing applied constant current (Fig. 4.4(a)) and/or electrolysis time. On the other hand, the distribution of silver was independent of the doping temperature, where the doping areas of Ag at 300, 400 and 500 °C were similar according to the SEM observation (Fig. 4.4(b)). These facts suggest that the rate of electrosubstitution in the glass can be controlled by electrical parameters such as the electric field or the current density rather than the doping temperature.

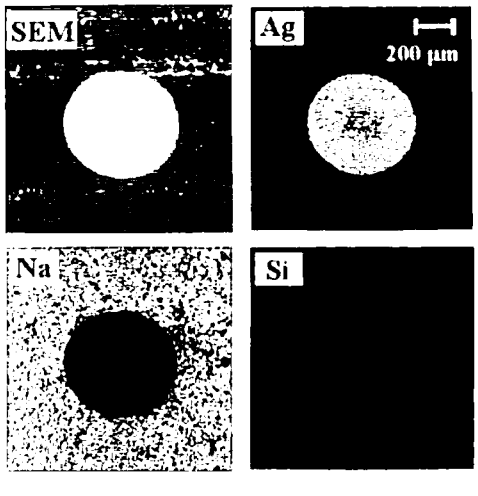

Figure 4.3. EPMA elemental maps of the anodic surface of Ag-doped glass. The doping was carried out at 10 μA for 60 min at 400 °C usitn the SOED 1 system.

The elemental distribution in the cross section of doped glass was also analyzed using EPMA. Figure 4.5 shows the time dependence on the distribution state of the dopant after 10 μA electrolysis at 400 °C. Notice that silver has already reached the glass / Na-β"-Al_2O_3 interface after 10 min electrolysis. Therefore, silver doping by the SOED method is a rapid process compared with the ion exchange method using a molten salt. Judging from Figs. 4.3 and 4.5, the distribution of silver occurs in a hemispherical shape in the glass. The distribution state of the dopant may be dominated by the potential distribution around the point contact electrode. The equipotential surface between the microelectrode and planar electrode will be constructed in a hemispherical configuration with its center at the microcontact [11-14]. Therefore, it is seen that Ag^+ radially diffused from the Ag-β"-Al_2O_3 / glass microcontact during the doping. As a result, hemispherical distribution of silver was obtained by this method.

To investigate the effect of the contact area at the cathodic side on the distribution of the dopant, the Ag doping into the glass was performed using a

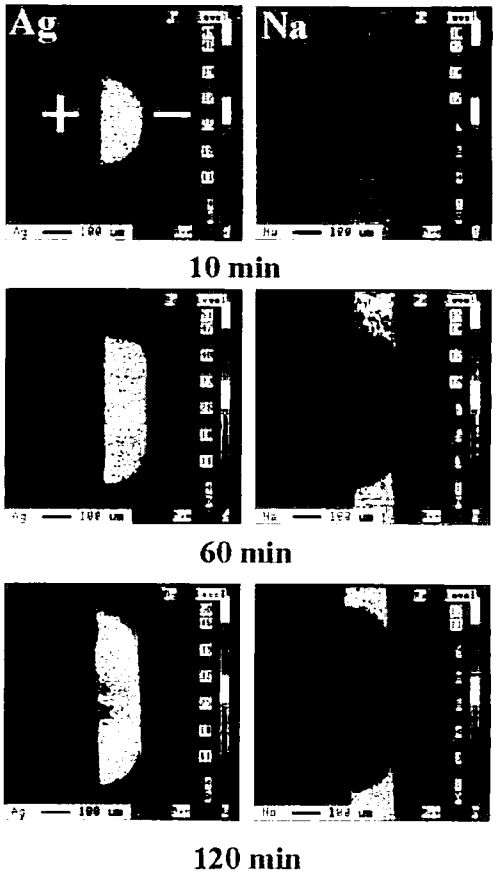

Figure 4.5. EPMA elemental distribution maps of the cross section of Ag-doped glass under 10 μA for various doping times.

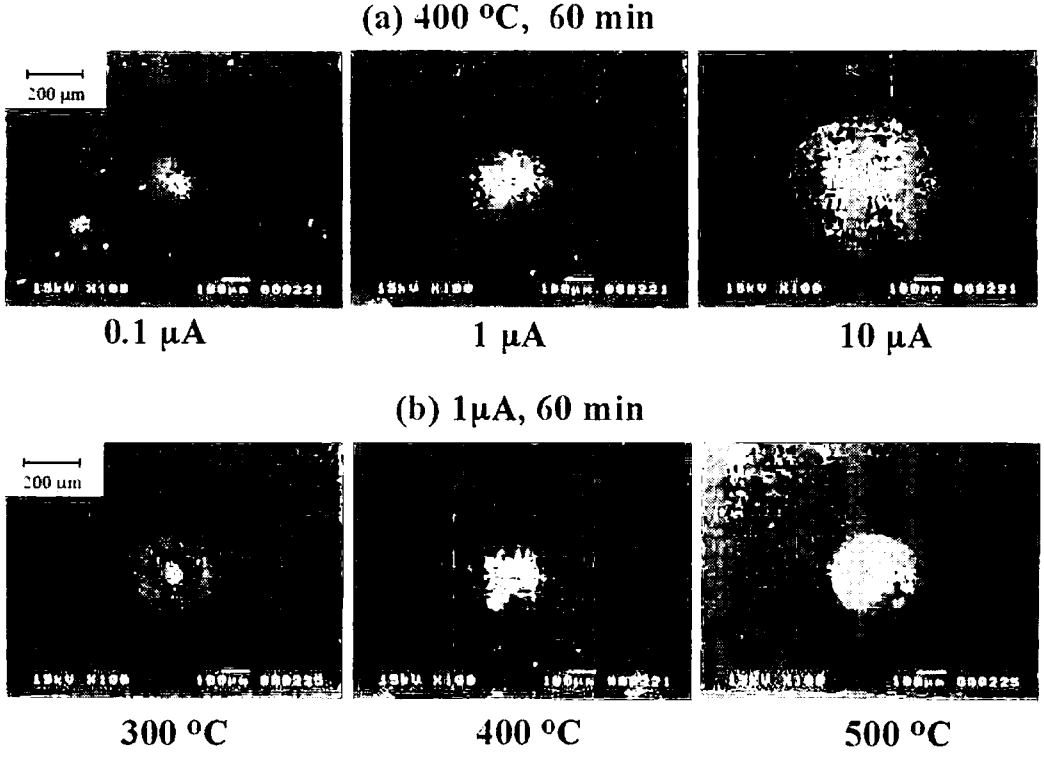

Figure 4.4. SEMs of the anodic surface of Ag-doped glass under various doping conditions. (a) Constant current dependence and (b) doping temperature dependence. Depression seen in the center of these images shows the Ag-β"-Al_2O_3 / glass microcontact.

Na-β"-Al_2O_3 microelectrode at the cathode side instead of a pellet sample in the SOED 1 system (Fig. 4.1(a)). Figure 4.6 shows the EPMA elemental distribution maps in the cross section of the Ag-doped borosilicate glass after applying 1 μA at 400 °C for 300 min. Replacing the planar cathode by a microelectrode reduces the diameter of the Ag distribution (about 140 μm), although a larger amount of electric charge was used. This result indicates that Ag^+ diffusion toward the parallel direction to the sample surface was suppressed by the cathodic side microcontact. Consequently, the distribution of dopant can be controlled by the contact area between β"-Al_2O_3 and the doping target as well as the current density or the doping time.

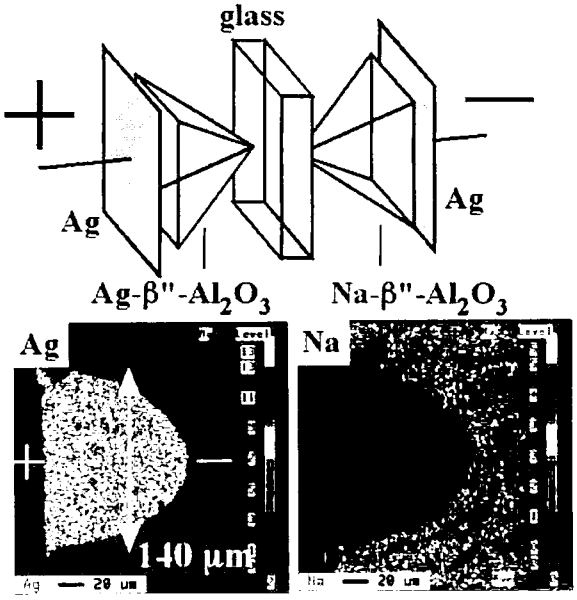

Figure 4.6. EPMA elemental distribution maps of Ag-doped glass after applying 1 μA for 300 min at 400 °C, where an Na-β"-Al_2O_3 microelectrode was used at the cathode side.

The pinpoint doping by the SOED method also depends on the valence of the dopant cation. Monovalent cations such as Ag^+, K^+ and Li^+ can be easily doped into the glass under an electric field. However, divalent cations such as Pb^{2+}, Ca^{2+} and Sr^{2+} can not be doped, since these dopants were deposited at the M-β"-Al_2O_3 / glass interface as its oxide or carbonate, or injected only into the surface region (< a few μm) [15]. The applied voltage under 1 μA at 400 °C for Pb^{2+} doping was about two orders of magnitude larger than that for the case of Ag^+, and reached about 10^3 V after 60 min. The applied voltage can somewhat reflect the degree of the migration rate in the glass, and will be small when the migration rate is large. The ionic conductivity of the monovalent cation in the glass is, for example, higher than that of the divalent one [16], because the divalent cation is more significantly affected than the monovalent cation by electrostatic interaction with the oxide ion in the glass.

Pinpoint doping into the BSCCO ceramics was carried out using a Na-β"-Al_2O_3 microelectrode. Figure 4.7 shows the applied voltage on the electrolysis time under constant current of 100 μA at 600 °C. (a) and (b) in this figure correspond to the cases of two SOED systems shown in Fig. 4.1, respectively. The applied voltage in the SOED 2 (b) was lower than that in the SOED 1 (a) during the electrolysis. A large voltage in the SOED 1 system (a) will be mainly based on the applied voltage for migration of Q^{m+} (in Fig. 4.1 (a)) in the BSCCO ceramics. The electrosubsitution of dopant for Q^{m+} in the BSCCO ceramics is difficult because this ceramics shows pure electron conduction but no significant ionic conduction, in contrast to

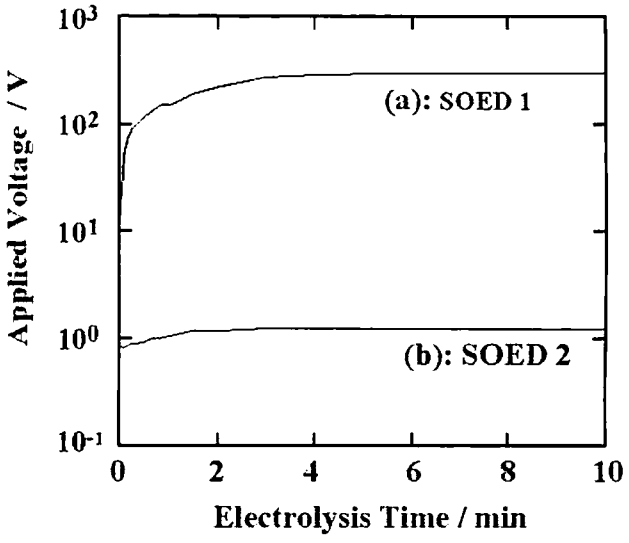

Figure 4.7. Dependence of the applied voltage on the electrolysis time for pinpoint Na doping the BSCCO ceramics.

the glass containing an alkali metal. On the contrary, the applied voltage in (b) shows the very small and constant value (about 1 V) suggests that the Na doping into BSCCO ceramics together with the injection of oxide ions from the YSZ proceed smoothly. In this case, Na^+ and O^{2-} migrate through the defects of ceramics (pore surfaces, grain boundaries etc.) [17]. This may be based on the higher ionic mobility in the grain boundaries than that of the grain bulk even though the total ionic conductivity is small. In principle, the cation doping using the SOED 2 (b) will proceed without any destruction of the crystal, since the doping occurs without cation substitution. Therefore, the SOED 2 (electro-bi-injection) may be more useful than the SOED 1 (electrosubstitution), when the substitution of the dopant cation in the doping target is difficult. Figure 4.8 shows the EPMA elemental distribution maps in the cross section of Na-doped BSCCO ceramics using the SOED 2 system after applying 100 μA for 60 min at 600 °C. This figure shows that the distribution of Na occurs in a hemispherical shape in the same manner as the silver doping into glass. According to the XRD patterns and EPMA elemental micromaps of doped ceramics, Na^+ was doped only into the grain boundaries as noted above.

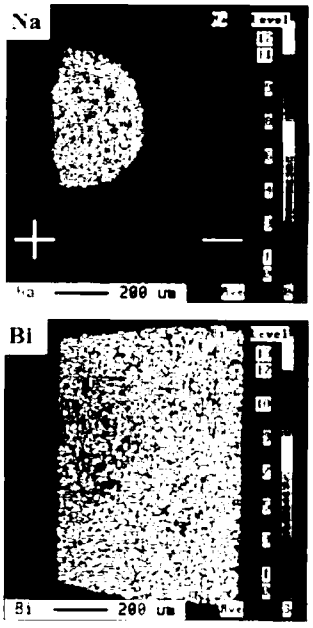

Figure 4.8. EPMA elemental maps of the cross section of Na-doped BSCCO ceramics using the SOED 2 system. The doping was carried out at 100 μA for 60 in at 600 °C.

4. 4. Conclusions

It should be noted that the pinpoint doping into the selected area of the borosilicate glass and BSCCO ceramics on a 10^2 μm scale was accomplished using the SOED method. The advisability of pinpoint doping was determined by the electrical property of the doping target and/or the valence of dopant. Thus, submicron ~ nanoscale doping may be possible if the contact radius of microelectrode and/or the electric charge are small. For practical purposes, the preparation of a photowaveguide in the glass matrix would be done by scanning the β"-Al_2O_3 anodic microelectrode during the doping. Hence, the pinpoint doping with a cation conducting microelectrode using the SOED method might become an important application with respect to solid electrolyte.

4. 5. References

[1] J. Fleig, S. Rodewald, J. Maier, *Solid State Ionics* **136-137**, 905 (2000).

[2] H.-D. Wiemhöfer, *Ber. Bunsenges. Phys. Chem.* **97**, 461 (1993).

[3] W. Zipprich, S. Waschilewski, F. Rocholl, H.-D. Wiemhöfer, *Solid State Ionics* **101-103**, 1015 (1997).

[4] G. Fafilek, *Solid State Ionics* **113-115**, 623 (1998).

[5] G. Fafilek, S. Harasek, *Solid State Ionics* **119**, 91 (1999).

[6] H. Rickert, H.-D. Wiemhöfer, *Ber. Bunsenges. Phys. Chem.* **87**, 236 (1983).

[7] S. Lübke, H.-D. Wiemhöfer, *Solid State Ionics* **117**, 229 (1999).
[8] R. Seevers, J. Denuzzio, G.C. Farrington, B. Dunn, *J. Solid State Chem.* **50**, 146 (1983).
[9] S. Sattar, B. Ghosal, M.L. Underwood, H. Mertwoy, M.A. Sartzberg, W.S. Frydrich, G.S. Rohrer, G.C. Farrington, *J. Solid State Chem.* **65**, 231 (1986).
[10] G.C. Farrington, B. Dunn, J.L. Briant, *Solid State Ionics* **3-4**, 405 (1981).
[11] J. Fleig, J. Maier, *Electrochim. Acta* **41**, 1003 (1996).
[12] J. Fleig, P. Pham, P. Sztulzaft, J. Maier, *Solid State Ionics* **113-115**, 739 (1998).
[13] J. Fleig, S. Rodewald, J. Maier, *Solid State Ionics* **136-137**, 905 (2000).
[14] U. Nigge, H.-D. Wiemhöfer, E.W.J. Römer, H.J.M. Bouwmeester, T.R. Schulte, *Solid State Ionics* **146**, 163 (2002).
[15] M.H. Shaaban, M.K. El Nimr, A.A. Ahmed, *J. Mater. Sci.* **4**, 208 (1993).
[16] M.H. Shaaban, A.A. Ahmed, A.R. Cooper, *Phys. Chem. Glasses* **40**, 34 (1999).
[17] G.S. Kulikov, R.SH. Malkovich, E.A. Skoryatina, V.P. Usacheva, T.A. Shaplygina, *Ferroelectrics* **144**, 61 (1993).

Chapter 5

Electrochemical Design of Metal Distribution in the Glass Using the SOED Method

5. 1. Introduction

Functional modification of glass surfaces is an effective method of imparting new characteristics to the original glass. [1] Well-established techniques include the deposition of films on the surface and the introduction of different elements into the surface region. For instance, silver or titanium coatings on the glass surfaces have already been used for IR-reflection or UV-cut glass. [2] The latter application corresponds to the ion-injection technique using gas phase ions at low pressure or ion-exchange using molten salts. Intended for use in conjunction with these methods, we recently proposed a new solid-state electrochemical route for introducing metal cations into glass using ion-conductors.[3] In this electrochemical approach, upon application of an electric field to the solid-solid interface between cation-conducting M-β"-Al_2O_3 and alkali metal ion containing glass, the metal cations (M^{n+}) are injected into the glass concurrently with the substitution for alkali metal cation in the glass. A significant advantage of this technique is that it enables pinpoint doping into the desired position in the glass with the aid of a β"-Al_2O_3 microelectrode, owing to which the contact radius of the solid-solid interface is typically about 10 μm. Indeed, we have already achieved pinpoint doping into alkali borosilicate glass and/or $Bi_2Sr_2CaCu_2O_y$ superconducting ceramics on a 10^2 μm scale using a β"-Al_2O_3 microelectrode as stated in Chpter 4. [4]

There have been recent reports on the application of the microelectrode technique to solid-state fabrication of metal micro- or nanostructures. Fleig et al. have reported on electromechanical writing of Ag microstructures (lines and letters) on the surface of a Ag^+-conducting AgCl single crystal, where cathodic deposition of Ag occurred selectively along the mechanical tracks scratched by a tungsten needle in advance.[5] Terabe et al. have prepared silver nanowires between a Ag_2S microanode and Pt cathode, set 1 nm apart from each other, by a cathodic solid-state electrochemical reaction where the Ag^+ ions arriving at the cathodic surface of Ag_2S react with the tunneling electrons generated from the Pt cathode under an electrical bias.[6] They mention that the fabricated Ag nanowires can easily dissociate by applying the reverse field, and that the formation-dissociation reactions can occur at a rapid field frequency of above 1 kHz. Iliescu et al. reported that silver-sweeping of α-quartz causes the growth of silver microwires inside the quartz crystals by electrodiffusion from the anodic $AgNO_3$ layer using tungsten microcathodes. [7] Our method would conceivably enable micropatterning of dopants in glass if the β"-Al_2O_3 microelectrode were to be moved along the glass surface during doping. The technique could be used to prepare optical devices, such as photowaveguides and microlenses, since pinpoint or patterned doping induces selective refractive index profiles in glass. In the present contribution, we have devised an electrochemical method for achieving metal cation distribution in the surface and interior of alkali silicate glass by manipulating a Ag-β"-Al_2O_3 microelectrode under an electric field.

5. 2. Experimental

Electrochemical cation doping was undertaken using the experimental setup schematized in Fig. 5.1(a). Ag-β"-Al_2O_3 was used as a Ag^+ conductor. The Ag-β"-Al_2O_3 microelectrode was prepared by the substitution of Ag for Na in Na-β"-Al_2O_3. A Na-β"-Al_2O_3 polycrystalline pellet (Nihon Tokushu Togyo Co.; thickness: 2 mm, diameter: 7 mm) was immersed in $AgNO_3$ molten salt for over 24 h. Electron probe microanalysis (EPMA) performed on the cross section of β"-Al_2O_3 revealed that the Na was completely exchanged. The resultant Ag-β"-Al_2O_3 was polished with emery paper to form a quadrangular pyramid-like microelectrode. Assuming a hemispherical microcontact between Ag-β"-Al_2O_3 and the doping target, the contact radius would typically be about 10 μm. An alkali silicate glass plate (12 Na_2O-1 K_2O-5 MgO-9 CaO-1 Al_2O_3-72 SiO_2 in mol%) was used as a doping target. Cation doping was performed at a constant current or voltage with a regulated DC power supply at 100 – 450°C in air, where the Ag-β"-Al_2O_3 microelectrode was scanned using a PC-operated, automated XYZ microstage (scan rate: 0 (fixed) ~ 1 mm/s). The change in applied voltage during electrolysis was monitored using a digital multimeter. It was checked that no doping occurred in the absence of the electric field at these temperatures. After doping, the distribution state of the dopant in the anodic surface and the cross section of the doping target was analyzed by EPMA.

5.3. Results and Discussion

The basic cation migration mechanism in the present system for pinpoint Ag doping into glass is illustrated in Fig. 5.1(b). Ag was electrochemically oxidized to Ag^+ at the Ag (anode) / Ag-β"-Al_2O_3 interface, and then injected into the glass. Na^+ migrated from the glass to the cathode side for maintenance of electrical neutrality in the glass. Na was deposited at the glass / Ag (cathode) interface and immediately reacted with the O_2 and CO_2 in air to form Na_2CO_3. [8] Hence, Ag^+ was substituted for Na^+ in the glass under an electrical field. [9] Thus, this doping scheme corresponds to an "electrosubstitution" mechanism.

Fig. 5.1(c) shows the optical micrographs of the anodic surface and the cross section of the glass (1 mm^3 cube) that was Ag-doped under a constant voltage of 30 V for 60 min at 400°C, where the Ag-β"-Al_2O_3 microelectrode was fixed onto the glass surface

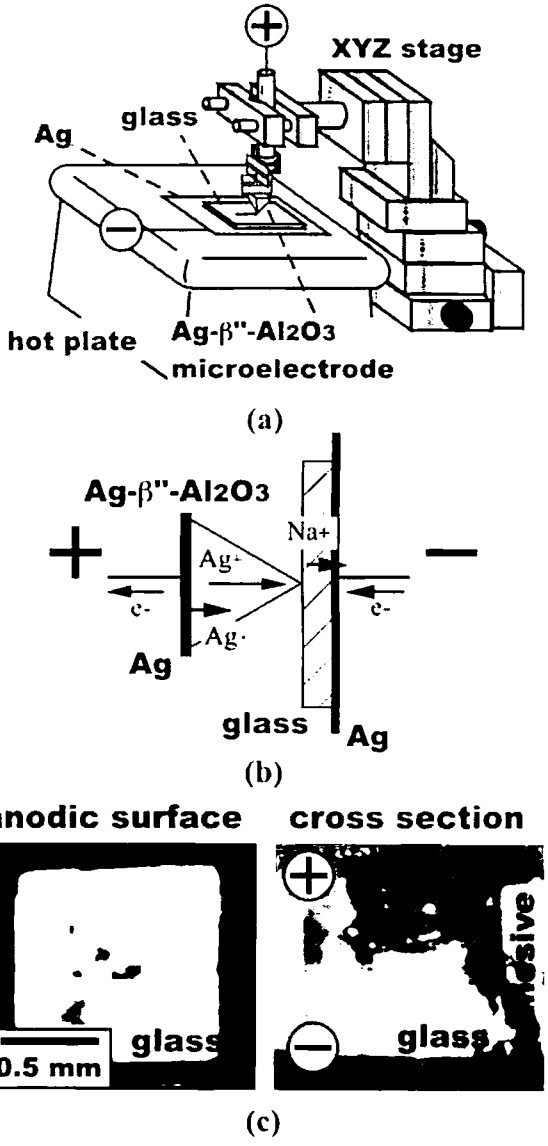

Figure 5.1. a) Experimental setup. b) the cation migration model of Ag doping using a Ag-β"-Al_2O_3 microelectrode, c) optical micrographs of the anodic surface and cross section of the glass after pinpoint Ag doping under constant voltage of 30 V at 400°C for 60 min.

during electrolysis (i.e., scan rate = 0 mm/s). It is believed that silver is present only in the concentrated areas in these micrographs, in the form of thermally produced Ag nanoparticles in the glass.[10] From our previous studies, [4] we know that the silver doping results in a hemispherical dopant distribution centered on the microcontact between β"-Al_2O_3 and the glass. In addition, the distribution diameter of the dopant on the anodic surface depended on the current density and/or the doping time, which reflect the amount of Ag doping.[11] The distribution state of the dopant may be dominated by the potential distribution around the point contact electrode. The equipotential surfaces between the microelectrode and the planar electrode exhibit a hemispherical shape with their center at the microcontact. [12] Thus, it can be concluded that Ag^+ diffused radially from the Ag-β"-Al_2O_3 / glass microcontact during doping. As a result, a hemispherical distribution of silver was obtained by this method. We have confirmed that various monovalent cations (K^+, Li^+, Cs^+) besides Ag^+ can be doped according to the same mechanism.

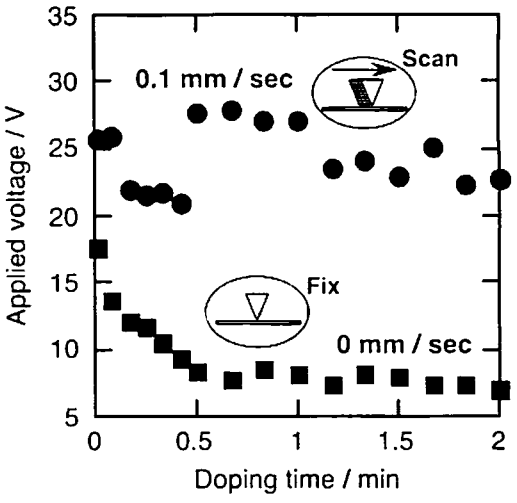

Figure 5.2. Time evolution of the applied voltage under a constant current of 10 μA at 200 °C with and witout tracing teh Ag-β"-Al_2O_3 microelectrode.

Fig. 5.2 shows the time evolution of applied voltage under a constant current of 10 μA at 200°C with and without tracing the Ag-β"-Al_2O_3 microelectrode along the glass surface. When the microelectrode was fixed on the glass surface, the applied voltage decreased rapidly during the initial stage of electrolysis (< 0.5 min) and remained at a nearly steady state after 0.5 min, corresponding to the slight voltage reduction. The effect of the cathodic Na_2CO_3 deposition, mentioned above in the description of the doping mechanism, on the total applied voltage can be neglected in the present method because the current density at the glass / Ag (cathode) interface would be negligible compared with that at the microcontact. Others have reported that the voltage response in the ion-conducting microelectrode technique depends on ionic conductivity only in the small region near the microcontact. [13] Taking into account the much larger ionic conductivity in Ag-β"-Al_2O_3 compared to that in the alkali glass, the voltage drop occurs mainly within the glass. Thus, the decrease in voltage under constant current suggests that the ionic conductivity in the glass around the microcontact increased with the substitution of Ag^+ for Na^+ in the silicate glass during the initial stage of electrolysis. This is mainly due to the higher ionic conductivity of Ag^+ in the amorphous glass network as compared to that of Na^+. [9, 14] By contrast, when the Ag-β"-Al_2O_3 was scanned during electrolysis, the applied voltage remained almost constant throughout the duration of electrolysis, except for some variations that may have been due to the temperature changes in the hot-plate set in ambient atmosphere. In this case, the Ag^+ injection always proceeded from the original glass surface, which contained only Na^+ as a charge carrier. That is, the chemical composition reflected by the ionic conductivity near the microcontact remained constant during doping.

EPMA elemental distribution maps of the anodic surface of Ag-doped glass with scanning an Ag-β"-Al_2O_3 microelectrode in a single direction at 130°C are shown in Fig. 5.3(a). The scan rates of the microelectrode were 1 mm/s (upper line) and 0.1 mm/s (lower line). These results indicate that Ag was dispersed in a line along the path of the microcontact, and that the line width was easily controlled by the electric charge per unit area, i.e., scan rate and/or current. According to the elemental distribution map of the cross section of the Ag-line drawn on glass, a semicircular Ag dispersion was observed, as in the case of the fixed microelectrode. Since the Ag-β"-Al_2O_3

microelectrode is attached to the automated XYZ stage (Fig. 5.1(a)), we can draw various silver patterns in the glass surface, not only simple structures (points and lines) but also more complicated forms (Fig. 5.3(b)). The lowest patterned Ag line width achieved to date is about 10 μm. However, the use of a microelectrode with a smaller contact radius and/or lower constant current (applied voltage) may enable the fabrication of finer and/or more complex patterns at the nanometer scale.

Expanding the present technique, we can control the glass composition not only in the surface region, but also in the bulk glass. In other words, the electrochemical design of glass composition is also possible in three dimensions. More specifically, following Ag patterning in the glass surface, Na^+ generated by the electrochemical decomposition of the Na_2CO_3 planar anode is re-injected into the Ag-doped glass in a direction that is parallel to the anodic surface as schematized in Fig. 5.3(c). EPMA elemental maps of the cross section of the rectangular glass (1 x 1 x 10 mm^3) containing the Ag distribution are shown in Fig. 5.3(d). In this case, first, Ag was doped using a fixed Ag-β"-Al_2O_3 microelectrode under 1 μA, for 60 min at 300°C. This was followed by Na^+ doping at 1 mA for 15 h at 400°C. Thanks to this two-step doping process, the Ag distribution is encapsulated within the glass sample by the Na^+ doping, during which it retains its hemispherical shape. It was found that the Ag concentration increased toward the direction of ion migration. Again, this is due to the larger ionic conductivity of Ag^+ in the glass compared with that of Na^+. As expected, the penetration depth of the Ag distribution depended on the electric charge of Na^+ doping in the second step. It was also confirmed that the line patterned Ag dispersion could exist only within the glass. Qiu et al. have substantiated the possibility of selectively inducing a change of valence state of metal ions on a micrometer scale inside a glass sample by the use of a focused pulsed laser.[15] By contrast, our electrochemical technique can cause a space-selective change of chemical composition inside the glass.

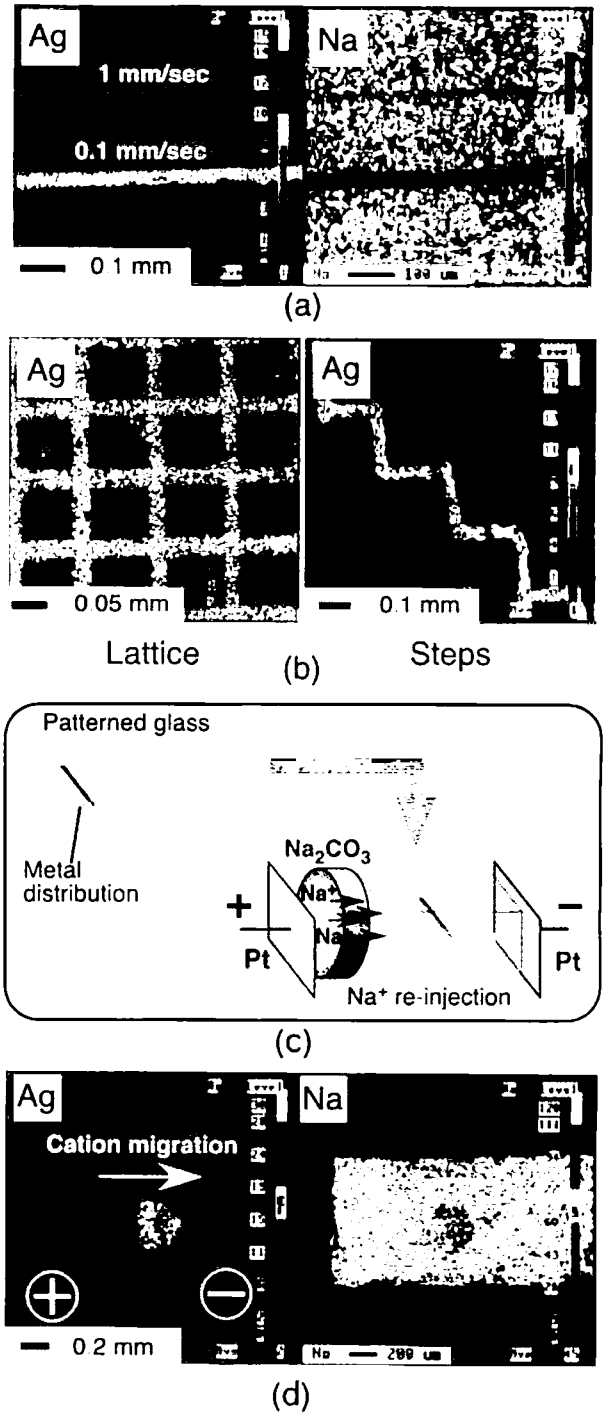

Figure 5.3. a) EPMA elemental distribution maps of the anodic surface Ag-doped glass with scanning the Ag-β"-Al_2O_3 microelectrode in a single direction 130 °C (scan rate: 1 mm/s (upper line and 0.1 mm/s (lower line)). b) More complex Ag patterns sketched in the glass surface. c) Schema of of a method for encapsulating the Ag-distribution inside the glass. d) Ag mapping after Na^+ re-injection at 1 mA and 400 °C for 15 h following pinpoint Ag doping at 1 μA and 300 °C for 60 min.

5. 4. Conclusions

In this communication, we have investigated the possibility of the electrochemical design of metal distribution in alkali silicate glass using a β"-Al_2O_3 microelectrode. Various patterns of Ag distribution were constructed near the surface or in the bulk. The size and shape of these patterns could be easily controlled by adjusting electrolysis conditions. The patterning of a metal distribution in the glass surface can also be achieved by ion-exchange in molten metal salts, a most effective and convenient method. However, multiple steps (masking to write a pattern, ion-exchange, washing, and etching of mask) have to be performed to obtain the desired structure.[16] Although the ion injection technique makes selective patterning possible by focusing the ion beam, it requires high energy (10^3-10^6 eV) for ion acceleration in a vacuum system, and the doping occurs only in the surface region of the substrate (<10^{-6} m). [17] By contrast, the present technique allows single step fabrication of patterned glass since various forms can be drawn directly via the solid-solid interface between β"-Al_2O_3 and glass under ambient atmosphere at a low-medium temperature range below the glass transition point. Furthermore, encapsulation of the metal distribution within the glass is one of the important features of the present electrochemical method. A variety of metal ion conducting solid electrolytes have been developed to date. Thus, this method can be employed to introduce many different kinds of metal ions into glass to impart it with new functions. The technique is expected provide a new and simple route for fabricating photowaveguides and/or microlens arrays; the optical characteristics of such optical devices built by this technique would help evaluate the effectiveness of the technique.

5. 5. References

[1] S. Tanaka, *Bull. Ceram. Soc. Jpn.* **1990**, *25*, 532.

[2] H. Murakami, *Bull. Ceram. Soc. Jpn.* **1995**, *30*, 677.

[3] Y. Matsumoto, *Solid State Ionics* **1997**, *100*, 165.

[4] a) K. Kamada, S. Udo, Y. Matsumoto, *Electrochem. Solid-State Lett.* **2002**, *5*, J1. b) K. Kamada, S. Udo, S. Yamashita, Y. Matsumoto, *Solid State Ionics* **2002**, *146*, 387.

[5] A. Spangenberg, J. Fleig, J. Maier, *Adv. Mater.* **2001**, *13*, 1466.

[6] a) K. Terabe, T. Hasegawa, T. Nakayama, M. Aono, *RIKEN Review* **2001**, *37*, 7. b) K. Terabe, T. Nakayama, T. Hasegawa, M. Aono, *Appl. Phys. Lett.* **2002**, *80*, 4009. c) K. Terabe, T. Nakayama, T. Hasegawa, M. Aono, *J. Appl. Phys.* **2002**, *90*, 10110.

[7] I. Enculescu, B. Iliescu, V. Teodorescu, *Solid State Ionics* **2001**, *138*, 315.

[8] Y. Matsumoto, K. Akagami, K. Kamada, *J. Solid State Chem.* **1999**, *143*, 111.

[9] C. Thévenin-Annequin, M. Levy, T. Pagnier, *Solid State Ionics* **1995**, *80*, 175.

[10] a) M.A. Villegas, J.M. Fernandez Navarro, S.E. Paje, J. Llopis, *Phys. Chem. Glasses* **1996**, *37*, 248. b) M. Antonello, G.W. Arnold, G. Battaglin, R. Bertoncello, E. Cattaruzza, P. Colombo, G. Mattei, P. Mazzoldi, F. Trivillin, *J. Mater. Chem.* **1998**, *8*, 457.

[11] K. Kamada, S. Udo, S. Yamashita, Y. Tsutsumi, Y. Matsumoto, *Solid State Ionics*, to be submitted.

[12] a) J. Fleig, J. Maier, *Electrochim. Acta* **1996**, *41*, 1003. b) J. Fleig, P. Pham, P. Sztulzaft, J. Maier, *Solid State Ionics* **1998**, *113-115*, 175. c) J. Fleig, S. Rodwald, J. Maier, *Solid State Ionics* **2000**, *136-137*, 905.

[13] a) H.-D. Wiemhöfer, *Ber. Bunsenges. Phys. Chem.* **1993**, *97*, 461. b) W. Zipprich, S. Waschilewski, F. Rocholl, H.-D. Wiemhöfer, *Solid State Ionics* **1997**, *101-103*, 1015.

[14] K. Matushita, M. Ito, K. Kamiya, S. Sakka, *Yogyo-Kyokai-Shi* **1976**, *84*, 496.
[15] a) J. Qiu, C. Zhu, T. Nakaya, J. Si, K. Kojima, F. Ogura, K. Hirao, *Appl. Phys. Lett.* **2001**, *79*, 3567. b) K. Miura, J. Qiu, S. Fujiwara, S. Sakaguchi, K. Hirao, *Appl. Phys. Lett.* **2002**, *80*, 2263. c) J. Qiu, M. Shirai, T. Nakaya, J. Si, X. Jiang, C. Zhu, K. Hirao, *Appl. Phys. Lett.* **2002**, *81*, 3040.
[16] C. R. Lavers, K. Itoh, S. C. Wu, M. Murabayashi, I. Mauchline, G. Stewart, T. Stout, *Sens. Actuators* **2000**, *B 69*, 85.
[17] G. Dearnaley, *Ion Implantation*, North-Holland, Amsterdam **1973**.

Chapter 6

Quantitative Assessment of the SOED Method

6. 1. Introduction

Functional improvements in various oxide ceramics have been accomplished using SOED. For example, in superconducting $YBa_2Cu_3O_y$ ceramics, selective silver doping only into the grain boundaries raises the critical temperature even for extremely small amount of doping (< 0.1 wt%) [1, 2]. Moreover, SOED is useful for pinpoint doping into the desired position within a material, provided the contact area between β"-Al_2O_3 and the doping target remains small during electrolysis [3, 4]. In particular, doped areas can be precisely controlled by passing a current through β"-Al_2O_3 microelectrodes, since the microcontact yields a homogeneous solid-solid interface.

The fact that the amount of dopant can be easily controlled by the total electric charge during electrolysis is regarded as another advantage of the SOED method. In the present study, the current efficiencies of cation doping by SOED were estimated based on the relationship between the dopant amount and the applied electric charge during electrolysis using Faraday's law. This allowed a quantitative assessment of cation doping by SOED. In this section, we have demonstrated that SOED is effective in controlling the dopant amount on a μmol-scale with high accuracy.

6. 2. Experimental

Electrochemical doping was carried out using the two types of setup shown in Fig. 4.1, where the M-β"-Al_2O_3 and Y-stabilized zirconia (YSZ) were used as cation and oxide ion conductor, respectively. We have used a M-β"-Al_2O_3 (M = Ag. Na) microelectrode as cationic source in order to avoid any inhomogeneous current flow at the interface between β"-Al_2O_3 and doping target. The Ag-β"-Al_2O_3 microelectrode was prepared by the substitution of Ag for Na in Na-β"-Al_2O_3 [5-7]. A Na-β"-Al_2O_3 polycrystalline pellet (Nihon Tokusyu Togyo Co.; thickness: 2 mm, diameter: 7 mm) was immersed in $AgNO_3$ molten salt at 553 K for longer than 24 h. The resultant β"-Al_2O_3 was polished with emery paper to form a quadrangular, pyramid-like microelectrode. A sodium borate glass (28 mol% Na_2O – 72 mol% B_2O_3; thickness: 0.7 mm), which was prepared by the conventional melt-quench method [8], and $Bi_2Sr_2CaCu_2O_y$ ceramics (BSCCO, Dowa Kogyo Co. Ltd.; thickness: 0.7 mm) were used as doping targets. The SOED 1 (Fig. 4.1(a)) and SOED 4.2 (Fig. 1(b)) systems were employed for cation doping into the glass and the BSCCO ceramics, respectively. Cation doping was performed at a constant current with a regulated DC power supply at 400 – 600 °C in air. No doping occurred in the absence of the electric field at these temperatures. After doping, the distribution of the dopant and the crystal structure of the doped sample were analyzed by EPMA (JEOL, JXA-8900) and XRD (using Cu-K_a radiation, Rigaku RINT-2500V), respectively. The doping amount of metal cation was estimated with an induced coupling plasma spectrometer (ICP, Nippon Jarrell Ash, IRIS Advantage) after dissolving the doped glass and BSCCO ceramics in aqueous HNO_3 solution.

6. 3. Results and discussion

Cation doping using β"-Al_2O_3 microelectrodes has been known to result in a hemispherical dopant distribution centered around the microcontact between β"-Al_2O_3 and the doping target, regardless of the electrolysis system (SOED 1 and 2) and the kind of the target materials (glass, ceramics, etc.) used [4]. Figure 6.1 shows the doping time dependence of the distribution radius of silver in Ag-doped sodium borate glass at a constant current of 10 μA at 400 °C, estimated based on the EPMA elemental distribution maps of the anodic surface of doped glass. The radius of the hemisphere was independent of doping temperature [3], but rather depended on the applied electric charge, which reflects the electrolysis time under galvanostatic conditions. That the radius of dopant distribution can be controlled by the electric charge suggests the doping amount may also be controllable by SOED.

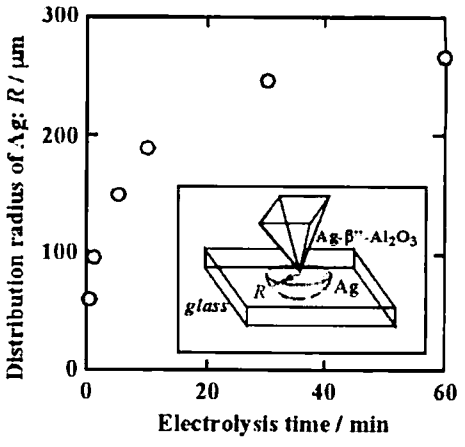

Figure 6.1. Time dependence of distribution radius (R) of Ag in glass at a constant current of 10 μA and 400 °C. Inset shows a schema of the Ag distribution in the glass.

6. 3. 1. Ag doping into sodium borate glass

We first evaluated the current efficiencies of Ag-doping into sodium borate glass. Figure 6.2 shows the typical change observed in applied voltage (a) and the amount of Ag doping into sodium borate glass (b) as a function of doping time at 10 μA and 400 °C. The solid line indicates the theoretical amount of Ag doping calculated based on Faraday's law. The applied voltage decreased sharply during the initial stage of electrolysis (< 10 min) and remained roughly constant after 10 min. Others have reported that the voltage response in the ion-conducting microelectrode technique depends on ionic conductivity only in the small region near the microcontact [9-11]. Therefore, the voltage change shows that the ionic conductivity around the microcontact increased with the substitution of Ag^+ for Na^+ in the borate glass during the initial stage of electrolysis. This is mainly due to the higher ionic conductivity of Ag^+ in the amorphous glass network as compared to Na^+ [12]. That the Ag amount increases linearly with doping time indicates that electrolysis time is an important factor for the control of dopant amount under galvanostatic conditions.

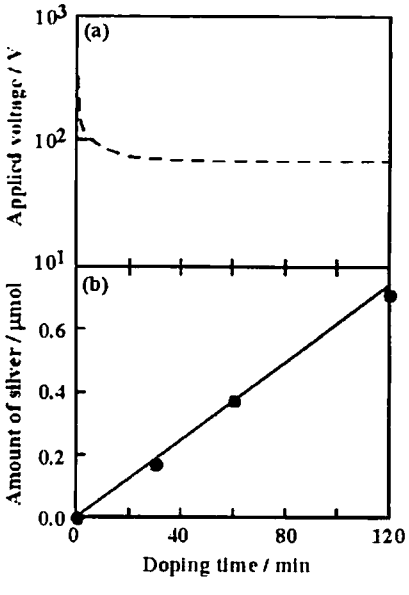

Figure 6.2. Doping time dependence of the applied voltage (a) and the amount of Ag dopant (b) during Ag doping into alkali borate glass at a constant current of 10 μA at 400 °C.

Table 6.1 lists the quantitative analysis results for Ag-doped glass and Faraday efficiencies of Ag-doping at a constant current of 10 μA at 400 °C for various doping times. The current efficiencies for Ag doping, calculated from the electric charge and the amount of Ag using Faraday's law, were above 90 %. This means that the amount of Ag doping can be easily controlled on a μmol scale by the electric charge during electrolysis. The high Faraday efficiencies in Ag-doping are due to the pure alkali cation conduction in the alkali borate glass because the alkali metal cations are easily substituted by Ag^+ during electrolysis [13].

Table 6.1. Quantitative analysis of Ag-doped glass and Faraday efficiency of Ag-doping at a constant current of 10 μA at 400 °C.

Doping time (min)	Measured Ag amount (μmol)	Calc. Ag amount[a] (μmol)	Current efficiency (%)
0[b]	< 0.001	0	———
30	0.174	0.187	93.0
60	0.376	0.373	101
120	0.715	0.746	95.8

[a]Calculated amount using Faraday's law.
[b]This glass was annealed at 673 K for 120 min while in contact with the Ag-β"-Al_2O_3 microelectrode under no electrical bias.

6. 3. 2. Na doping into superconducting BSCCO ceramics

We have also investigated the quantitative aspects of Na-doping into BSCCO ceramics using Na-β"-Al_2O_3 microelectrodes. The SOED 2 system (electro-bi-injection) was employed because the electrosubstitution of cations was difficult in an electron conducting ceramics. Figure 6.3 shows the typical applied voltage (a) and the amount of Na doping into BSCCO ceramics (b) as a function of doping time at 10 μA and 100 μA at 600 °C. The solid lines indicate the theoretical amount of Na doping calculated from Faraday's law. At a constant current of 10 μA, the Na dopant amount increased linearly with doping time, in a similar fashion to Ag-doping into glass. However, the amount of Na detected at 100 mA was in excess of the theoretical value. XRD analysis of the anodic surface of Na-doped BSCCO ceramics (100 μA, 30 min) revealed deposition of Na_2CO_3 at the interface between the Na-β"-Al_2O_3 microelectrode and the ceramics.

Table 6.2 lists the quantitative analysis results for Na-doped BSCCO ceramics and the corresponding Faraday efficiencies at a constant current of 10 μA and 100 μA at 600 °C for various doping times. Although Faraday efficiencies of Na-doping into BSCCO at 10 μA were lower compared with Ag-doping into glass, relatively high efficiencies of above 80 % were obtained. In Na-doping into BSCCO ceramics using SOED 2, Na^+ exists as Na_2CO_3 [4, 14], and can be doped only into structural defects (grain boundaries and/or pore surfaces) because these defects provide the fastest diffusion path for the mobile ions [15, 16]. Thus, the current efficiencies of Na-doping were reduced since the grain boundaries with limited volume became saturated with Na_2CO_3. This phenomena is reflected in the gradual increase in the applied voltage during the initial stage of doping as shown in Fig. 6.3(a). In

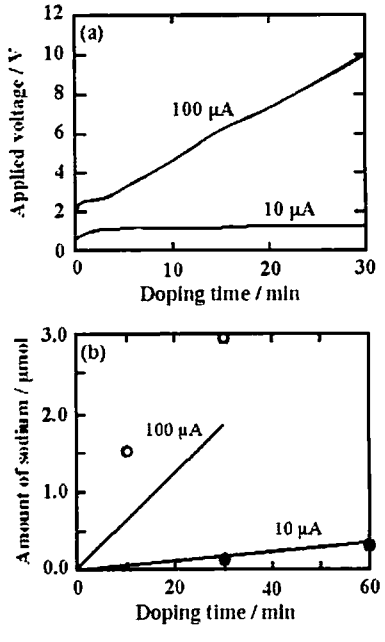

Figure 6.3. Doping time dependence on the typical applied voltage (a) and the doping amount of sodium (b) in the case of Na-doping into the BSCCO ceramics at a constant current of 10 μA or 100 μA at 600 °C

this case, the leakage current may be due to the electron conduction through the superconducting ceramics.

On the other hand, Na excess in BSCCO ceramics at 100 μA will primarily originate in the Na_2CO_3 deposits on the ceramics as stated above. Under the experimental conditions, the current density through the microcontact is extremely large (> 10 Acm^{-2}), because the contact radius between the β"-Al_2O_3 microelectrode and the ceramics is about 10 μm. Changes (compositional and/or crystal structural) in the electrolyte may occur near the point contact electrode because the local electric field may attain a relatively high value [17]. Therefore, the temperature around the microcontact is expected to increase with the current-induced Joule heat. The increase in temperature may cause the thermal diffusion of Na from Na-β"-Al_2O_3 to the BSCCO ceramics, where the Na^+ will be deposited at the anodic interface. In conclusion, current efficiencies of Na-doping into BSCCO ceramics depend on the current density during electrolysis. More specifically, Na-doping quantitatively proceeds at low current densities, while an excess Na is detected on the anodic surface at high current densities.

Table 6.2. Results of quantitative analysis of Na-doped BSCCO ceramics and Faraday efficiency of Na-doping at a constant current of 10 μA or 100 μA at 600 °C.

Doping condition	Measured Na amount (μmol)	Calc. Na amount[a] (μmol)	Current efficiency (%)
10 μA, 30 min	0.149	0.187	79.7
10 μA, 60 min	0.345	0.373	92.5
100 μA, 10 min	1.529	0.622	246
100 μA, 30 min	2.949	1.865	158

[a]Calculated amount using Faraday's law.

6. 4. Conclusions

A quantitative analysis of cation doping by SOED was performed. For Ag-doping into alkali borate glass, the measured doping amount almost exactly matched the theoretical value calculated from Faraday's law. That high current efficiency values of above 90 % were obtained suggests that the dopant amount can be precisely controlled on a μmol scale by adjusting the electric charge during electrolysis. Current efficiencies of Na-doping into BSCCO ceramics depended on the applied constant current. We achieved efficiencies of above 80 % at a constant current of 10 μA. These relatively low efficiencies were attributed to the saturation of BSCCO grain boundaries with the Na dopant. Excess Na was detected on the anodic surface of the BSCCO at a constant current of 100 μA because of the thermal diffusion of Na due to the current-induced Joule heat.

Conventional techniques for the introduction of metal cations into glass surfaces are (i) ion-exchange using molten salts and (ii) ion-injection using gas phase ions at low pressure. It is difficult to control the amount of metallic dopant by these methods. One major advantage of the SOED method is that it enables the precise control of dopant amount using ion-conducting β"-Al_2O_3 microelectrodes. Furthermore, the doped area on the glass surface could be micropatterned by scanning the β"-Al_2O_3 anodic microelectrode during doping. Thus, the proposed SOED technique may be utilized for fabricating photowaveguides in glass matrices. Hence, SOED may well become one of most important applications with respect to solid electrolytes.

6. 5. References

[1] Y. Matsumoto, M. Koinuma, H. Yamamoto, T. Nishimori, *Solid State Ionics* **95**, 309 (1997).

[2] Y. Matsumoto, *J. Solid State Chem.* **128**, 93 (1997).

[3] K. Kamada, S. Udo, S. Yamashita, Y. Matsumoto, *Solid State Ionics* **146**, 387 (2002).

[4] K. Kamada, S. Udo, Y. Matsumoto, *Electrochem. Solid-State Lett.* **5**, J1 (2002).
[5] R. Seevers, J. Denuzzio, G.C. Farrington, B. Dunn, *J. Solid State Chem.* **50**, 146 (1983).
[6] S. Sattar, B. Ghosal, M.L. Underwood, H. Mertwoy, M.A. Sartzberg, W.S. Frydrich, G.S. Rohrer, G.C. Farrington, *J. Solid State Chem.* **65**, 231 (1986).
[7] G.C. Farrington, B. Dunn, J.L. Briant, *Solid State Ionics* **3-4**, 405 (1981).
[8] H. Itoigawa, T. Kamiyama, Y. Nakamura, *J. Non-Cryst. Solids* **220**, 210 (1997).
[9] J. Fleig, J. Maier, *Electrochim. Acta* **41**, 1003 (1996).
[10] H.-D. Wiemhöfer, *Ber. Bunsenges. Phys. Chem.* **97**, 461 (1993).
[11] W. Zipprich, S. Waschilewski, F. Rocholl, H.-D. Wiemhöfer, *Solid State Ionics* **101-103**, 1015 (1997).
[12] K. Matusita, M. Ito, K. Kamiya, S. Sakka, *Yogyo-Kyokai-Shi* **84**, 496 (1976).
[13] C. Thévenin-Annequin, M. Levy, T. Pagnier, *Solid State Ionics* **80**, 175 (1995).
[14] Y. Matsumoto, K. Akagami, K. Kamada, *J. Solid State Chem.* **143**, 111 (1999).
[15] G.S. Kulikov, R.SH. Malkovich, E.A. Skoryatina, V.P. Usacheva, T.A. Shaplygina. *Ferroelectrics* **144**, 61 (1993).
[16] T.D. Dzhafarov, H. Comert, M. Altunbas, U. Alver, T. Kucukomeroglu, A.I. Kopya, *J. Alloys Compds.* **221**, 264 (1995).
[17] B. Gharbage, F.M.B. Marques, J.R. Frade, *Solid State Ionics* **136-137**, 933 (2000).

Chapter 7

General Conclusions

In this thesis, we have proposed a new electrochemical doping method using solid electrolytes, i.e., Solid Oxide Electrochemical Doping (SOED), and elucidated the doping mechanism of the SOED method in detail. As a result, the following important information was obtained.

Some experimental results of SOED 1 are shown in Chapter 2. The results indicate that SOED 1 is a very useful method for doping various cations into all of the functional oxide ceramics independent of their conductive properties. In general, the doping occurred only in the grain boundaries at a small current density or low applied voltage, while the doping sometimes occurred in the bulk of the grains (crystal lattice) at a high current density or high applied voltage. As a matter of course, the doping point strongly depends on the kind of ceramics (crystal structure, grain size, etc.) and the dopant (ionic size, valence, etc.). Moreover, an improved system of SOED 1 to dope trivalent ions, which was difficult to incorporate to β"-Al_2O_3 structure, was demonstrated. Bi-doped ZnO ceramics prepared by this technique shows the significant varistor characteristics, and its properties were simply controlled by the doping condition. According to the study about the anodic reaction of metal or metal compound / Na-β"-Al_2O_3 interface, it was proved that some metal or metal carbonate is appropriate as an anode in the SOED system.

Electrochemical cation doping into oxide ceramics has been studied using the SOED 2 (electro-bi-injection) in Chapter 3. In the SOED 2, the metal cation M and oxide ion are simultaneously injected into the oxide ceramics so that electrical neutrality is maintained in the ceramics. In general, graded doping occurred independent of the conductivity type of the oxide ceramics at relatively high temperature, because the migration rate of the oxygen anions is close to that of the metal cation in the grain boundaries of the ceramics at high temperature. As a result, the metal cation was graded on the anode side of the oxide ceramics. However, doping is too difficult at low temperature because the migration of oxygen anions is much faster than that of the cations at low temperature. As expected, doping results depended on the valence of the doped cation.

In Chapter 4, pinpoint metal cation doping was carried out using the SOED method, where a microelectrode of M-β"-Al_2O_3 as the solid electrolyte was used as a cationic source. Two different electrolysis systems (SOED 1 and 2) were employed. The pinpoint doping strongly depends on the conductive properties of the doping target and the valence of the dopant cation. Therefore, the cation doping into the alkali borosilicate glass occurs using only the SOED 1 system, because the glass shows a pure cationic conduction. In contrast, a cation can be doped into the superconducting $Bi_2Sr_2CaCu_2O_y$ ceramics using only the SOED 2 system because the electrosubstituion of a cation was difficult in an electron conducting ceramics. In this case, the migration of the metal cations and the oxide ions primarily proceeds through the defects of ceramics (pore surfaces, grain boundaries etc.). The fact, that the pinpoint distribution of the dopant can be controlled by the contact area between the microelectrode and the doping target, indicates the migration of dopant was dominated by the potential distribution in the target materials under an electric field. As a result, we have achieved pinpoint doping on a 10^2 μm scale using the SOED method.

In Chapter 5, electrochemical design of metal distribution on the alkali borosilicate glass was carried out using an ion-conducting microelectrode. When the Ag-β"-Al_2O_3 microelectrode was fixed onto the glass surface, the distribution of silver occurred in a hemispherical shape with its center at the Ag-β"-Al_2O_3 / glass microcontact. The diameter of the Ag-doped area strongly depended on the applied electric charge which reflects the amount of Ag doping. On the other hand, scanning Ag-β"-Al_2O_3 microelectrode under applying an electric field caused the patterned Ag-distribution in the glass surface so that the contact radius between Ag-β"-Al_2O_3 and glass was extremely small (< 10 μm).

Quantitative analysis of metal cation doping by the SOED has also been performed under galvanostatic doping conditions. A M-β"-Al_2O_3 (M= Ag, Na) microelectrode was used as cation source in order to attain a homogeneous solid-solid contact between the β"-Al_2O_3 and doping target. In Ag-doping into alkali borate glass, the measured dopant amount closely matched the theoretical value. High Faraday efficiencies of above 90% were obtained. This suggests that the dopant amount can be precisely controlled on a mmol scale by the electric charge during electrolysis. On the other hand, current efficiencies of Na-doping into $Bi_2Sr_2CaCu_2O_y$ (BSCCO) ceramics depended on the applied constant current. Efficiencies of above 80 % were achieved at a constant current of 10 μA. The relatively low efficiencies for Ag-doping into glass were explained by the saturation of BSCCO grain boundaries with Na. By contrast, excess Na was detected on the anodic surface of ceramics at a constant current of 100 μA as a result of the thermal diffusion of Na due to the current-induced Joule heat. In the present study, we demonstrate that SOED enables μmol-scale control over dopant amount. These results were noted in Chapter 6.

Consequently, the SOED method, especially SOED 1 and 2, allow for a micro-area doping in the ceramics, if the contact area between solid electrolyte and doping target is small. Moreover, the graded materials in the dopants (for example, optical glass, etc.) may be made with the SOED methods, when the doping time is very short (for example, by a pulse electrolysis technique). These techniques are very important for the development of the electroceramics used in microelectronics, and are impossible by the previously stated conventional doping method. The SOED method is expected as an important application with respect to solid electrolytes in the near future.

List of Publications

Chapter 2

Y. Matsumoto, T. Nishimori, H. Yamamoto, K. Nishimuira, K. Kamada, A. Ogata, "Calcium Doping into the $YBa_2Cu_3O_y$ Ceramics by the SOED Method", *Solid State Ionics*, **107**, 41 (1998).

Y. Matsumoto, K. Akagami, K. Kamada, " Electrosubstitution at the Metal, Metal Compounds / Na-β"-Al_2O_3 Interface in the SOED Method", *J. Solid State Chem.*, **143**, 111 (1999).

Y. Matsumoto, K. Kamada, Y. Tanaka, "Bismuth Doping into the ZnO Ceramics Using the SOED Method", *Chem. Mater.*, **11**, 3018 (1999).

K. Kamada, Y. Yanaru, Y. Matsumoto, "Cation Doping into the Superconducting Bi-Sr-Ca-Cu-O Ceramics Using the Solid Oxide Electrochemical Doping Method", *Electrochemistry*, **68**, 540 (2000).

Chapter 3

K. Kamada, Y. Matsumoto, "Cation Doping of Oxide Ceramics Using Solid Oxide Electrochemical Doping: Evaluation of the SOED 2 Method", *J. Solid State Chem.*, **146**, 406 (1999).

Chapter 4

K. Kamada, S. Udo, Y. Matsumoto, "Pinpoint Silver Doping into Borosilicate Glass by Solid Oxide Electrochemical Doping", *Electrochem. Solid-State Lett.*, **5**, J1 (2002).

K. Kamada, S. Udo, S. Yamashita, Y. Matsumoto, "Pinpoint Doping Using a β"-Al_2O_3 Microelectrode as one Application of Solid Oxide Electrochemical Doping (SOED) Method", *Solid State Ionics*, **146**, 387 (2002).